Master's thesis

NTNU
Norwegian University of Science and Technology
Faculty of Engineering
Department of Geoscience and Petroleum

Patience Ankah

# Influence of silicate minerals on spontaneous imbibition of water within a porous medium.

Master's thesis in petroleum geoscience
Supervisor: Ole Torsæter
December 2019

NTNU
Norwegian University of
Science and Technology

Patience Ankah

# Influence of silicate minerals on spontaneous imbibition of water within a porous medium.

Master's thesis in petroleum geoscience
Supervisor: Ole Torsæter
December 2019

Norwegian University of Science and Technology
Faculty of Engineering
Department of Geoscience and Petroleum

NTNU
Norwegian University of
Science and Technology

.

# Acknowledgement

I thank the Almighty God for his grace and abundance of mercy during this project. I wish to thank the Department of Geoscience and Petroleum, Norwegian University of Science and Technology, for the opportunity to write this research (project). Special thanks goes to my supervisor, Prof. Ole Torsæter for his patience and support, Alberto Bila and Salem Akarri for their tremendous contributions during my laboratory experiment.

I wish to express my sincere gratitude, once again to Prof. Ole Torsæter for this encouragement and care during my pregnancy and postpartum while working on my thesis. I wish to thank my mother, Phyllis Geraldo who took care of the baby while i concentrate to complete my thesis.

# Abstract

Clastic (Sandstone) sedimentary rocks are proven to be about 60% of all the prolific petroleum reservoirs with its important petrophysical rock properties being porosity and permeability. However, the wetting condition of the rock affect the petroleum production. These petrophysical rock properties are strongly influenced by textural properties of the sediment. The vast majority of the minerals in sandstone sediments are silicate minerals.

This study investigates the effect silicate minerals have on spontaneous imbibition of water on core samples. Laboratory experiments and petrographical studies were conducted on four core samples. Evaluation of porosity, permeability, as well as wettability are information derived from routine/conventional and special core analysis. Porosity is calculated using Helium Porosimeter, permeability is measured from Constant Head Permeameter and the average wettability index of the various cores were determined using the Amott cell test. The identification of minerals in the rock samples were done by observing images of thin sections viewed under a polarizing microscope. By studying the samples under SEM detailed information about the unknown samples were obtained. Backscattered electron images (BEI) in combination with Energy Dispersive Spectrometer (EDS) were used to calculate the elemental composition and identification of the minerals.

It was found that samples with high amount of quartz minerals are proven to be water wet but not all water wet samples readily imbibe water.

# Table of Contents

# List of Tables

# List of Figures

# Nomenclature

| | | |
|---|---|---|
| A | = | Cross-sectional area [$cm^2$] |
| D | = | Diameter of core sample [cm] |
| k | = | Permeability [darcy] |
| L | = | Length of core sample [cm] |
| $\phi_e$ | = | Effective porosity [%] |
| $Q_{atm}$ | = | Flow rate [$cm^3/sec = mL/sec$] |
| $\mu$ | = | Viscosity of the flowing liquid [cP] |
| $(P_1^2 - P_2^2)$ | = | Differential pressure across the core [atm] |
| $P_{atm}$ | = | Atmospheric pressure [atm] |
| $P_m$ | = | The mean pressure [atm] |
| Vb | = | Bulk volume [$cm^3$] |
| Vg | = | Grain volume [$cm^3$] |
| Vp | = | Pore volume [$cm^3$] |
| $V_1$ | = | Volume of matrix cup without core [$cm^3$] |
| $V_2$ | = | Volume of matrix cup with core [$cm^3$] |
| $V_{o1}$ | = | volume of oil produced during water imbibition [mL] |
| $V_{o2}$ | = | volume of oil produced during water flooding [mL] |
| $V_{w1}$ | = | volume of water produced during oil imbibition [mL] |
| $V_{w2}$ | = | volume of water produced during oil flooding [mL] |

Chapter 1

# Introduction

## 1.1 Background

Prediction of porosity and permeability is very important in the reservoir quality analysis as well as pre drilling in the oil and gas industry. Empirical predictions of porosity and permeability of sandstone being the current trend/approach prior oil/gas drilling commences (Bloch, 1991). However, the preferential tendency of one fluid in the presence of another to adhere to a solid surface is of great interest.

The mineral and textural composition of sedimentary rock which is determined by packing of the grains, grain size and grain size distribution. This textural properties affect the storage capacity of the rock (porosity), transport capacity (permeability) and the relative flow of one fluid in a multiphase system (relative permeability) (Beard and Weyl, 1973; Niazia et al., 2019). The relative permeability is dependent on the wettability of the rock.
According to Amott (1959), wettability of porous rock can be described as preferentially water-wet or preferentially oil-wet. In some cases a third classification, neutral wettability, has been used.

Compaction and cementation are diagenetic processes that may alter the pore space in rocks especially sandstones. Formation damage caused by the presence of shale and the clay minerals found in shale impairs the quality of reservoir properties such as porosity and permeability. These reservoir properties are essential for efficient exploitation and recovery of hydrocarbon reserves, hence the presence the shale and clay minerals may cause economic

as well as undesirable operational problems.

### 1.1.1 Objectives

This project aims to investigate the wettability of sandstone with regards to the influence of mineralogy on the reservoir parameters especially wettability. The main objectives of the experimental work done during this project are:
(1) Determine the wettability of different core samples using the Amott Cell method as well as to estimate the petrophysical properties (porosity and permeability) of core samples and the effect of mineralogy on these properties.
(2) The identification of various minerals in the rock samples by observing images of thin sections viewed under a polarizing microscope.
(3) Studying the samples under Scanning Electron Microscope (SEM) to obtain detailed information about the unknown samples. This will be performed by using Backscattered electron images (BEI) in combination with Energy Dispersive Spectrometer (EDS) to calculate the elemental composition and to aid in the identification of the minerals.

## 1.2 Thesis Outline

The content of this thesis is grouped into six chapters with various sections and subsections where applicable:
-Introduction
-Basic theory
-Data set and methodology
-Results
-Discussion
-Conclusion and recommendation

Chapter 2

# Basic Theory

## 2.1 Rock Petrophysical properties

The most important physical properties of a reservoir rock are the ability of the rock to store fluids such as oil, gas and water, this is defined as the porosity and the transport ability of the rock defined as the permeability of a rock. Adequate knowledge of these two properties are important in fluid recovery estimates as well as the fluid flow rate. However, sandstone reservoirs are important hydrocarbon reservoirs in terms of their physical properties such as porosity and permeability, which depends on the processes that produces these sediments (Tiab and Donaldson, 2015).

### 2.1.1 Porosity

Porosity can be defined as the void spaces within a rock or the ratio of volume of pore to the bulk volume of a reservoir rock. Porosity can be expressed as a percentage or fraction of the bulk volume. It can mathematically be expressed as:

$$\phi = \frac{\text{Volume of pore space}}{\text{Bulk volume}} = \frac{Vp}{Vb}$$

The total or absolute porosity and effective porosity are the two types of porosity that can be measured.

**Total or absolute porosity** is defined as the volume of reservoir rock which is filled with

fluid (oil, gas and water), expressed as a percentage or fraction of the bulk rock volume. **Effective porosity** is defined as the ratio of the sum of all interconnected pore space to the the bulk rock volume.

The porosity of a formation can be estimated either from individual log reading; neutron, density, sonic, NMR or obtained from the combination of different logs eg. neutron-density crossplot or obtained from the laboratory by core sample analysis. However, porosities are estimated from the measured parameters (Bjørlykke, 2010).

Porosity can be classified as primary (original) or secondary depending on its origin. Primary porosity are formed or determined during time of deposition of sediment. This type of porosity are inherent characteristics of the rock. Secondary porosity caused by later changes the rock undergoes as a result of geological processes such as diagenesis after the deposition of sediment. This changes can either increase porosity through fracturing or dissolution process or decrease the original porosity as a result of cementation (Fraser, 1935; Torsæter and Abtahi, 2003).

### Factors Governing Porosity

Normally, the porosities of reservoir ranges from 5% to 30%. However, there are several factors turn to determine the magnitude of the porosities in clastic sediment. These factors include grain sorting or the uniformity of grain size, grain packing, grain shape (Sphericity) and roundness (Angularity) as shown in (**Fig. 2.1**).

Graton and Fraser (1935) have discussed that there are different types of packing depending upon the angle of intersection of the grain set of row in a layer. They have also shown that the cubic packing of same size, has higher porosity of 48% as compared to the others as shown in **Fig. 2.2**. However, cubic packing will two grain sizes where a smaller grain is introduced into the cubic packing, the porosity decreases. According to Fraser (1935), porosity increases as grain size decreases because of the higher surface ratio of surface area to volume and mass; as there is an increasing tendency towards friction, adhesion and bridging.

Another important factor is compaction and cementation. Reduction in the bulk volume (compaction) of the sandstone is the controlling mechanism of reduction of porosity in most sandstones as shown in **Fig. 2.3**. However, well sorted coarse grained sized sand tends have

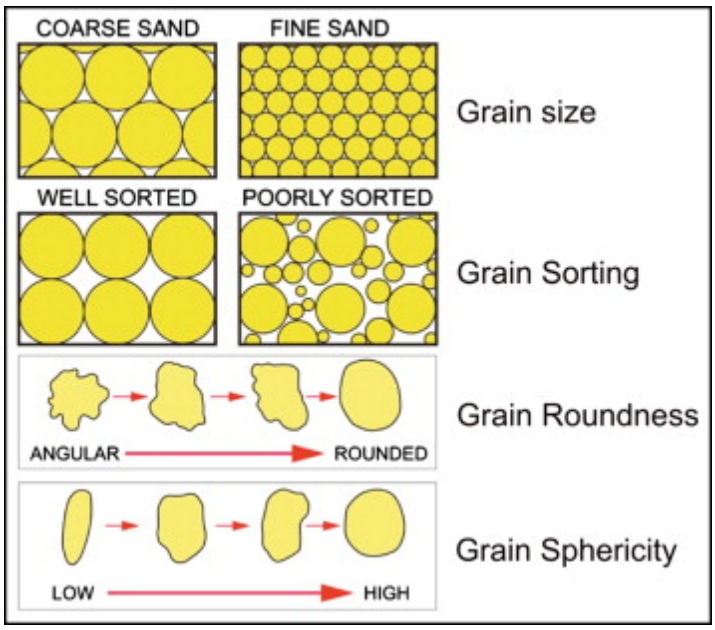


**Figure 2.1:** Textural properties of clastic sediments (Slatt, 2013).

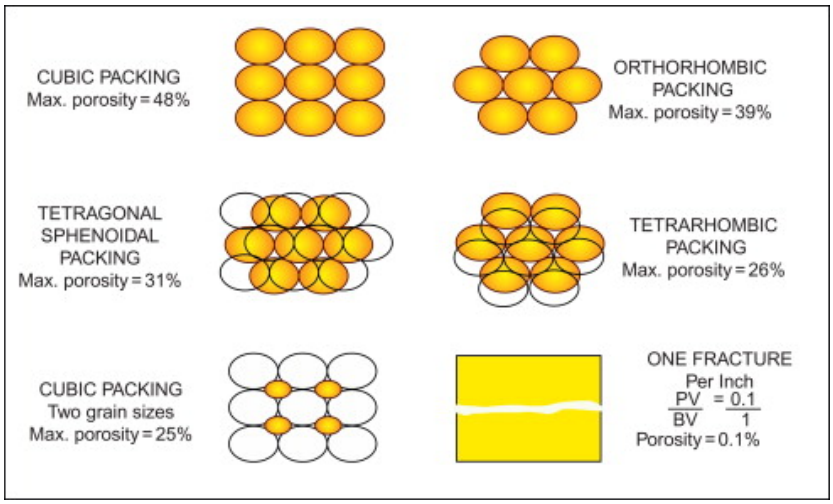


**Figure 2.2:** Effect of grain packing on porosity (Oyeneyin, 2015).

a more reduction in porosity during compaction because they are more compressible (Lander and Walderhaug, 1999). Quartz overgrowth are formed usually when quartz cement precipitate around the original grain of quartz. Coating of quartz grains during early diagenetic process helps to preserve primary porosity when the quartz grain is completely coated.

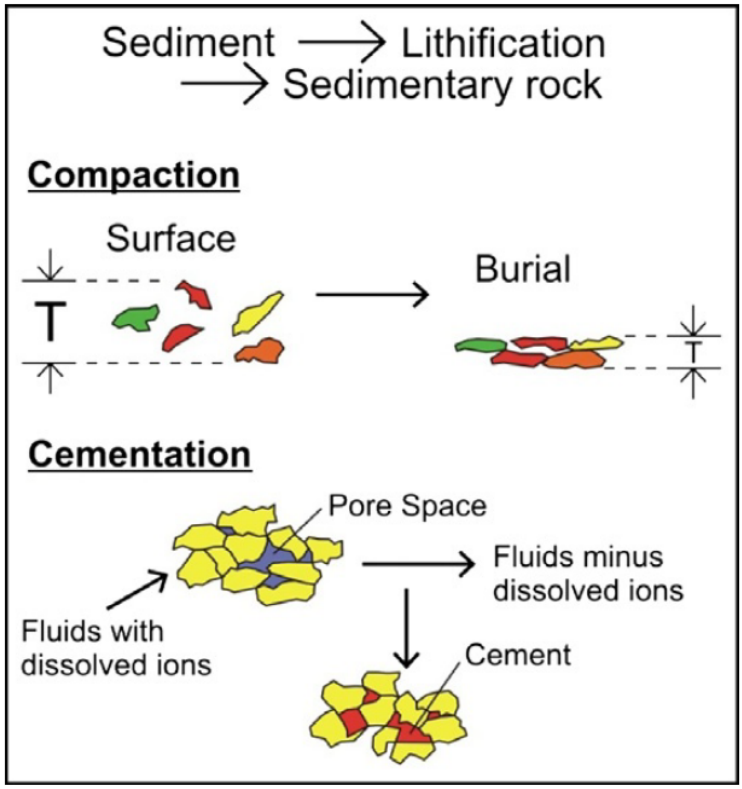


**Figure 2.3:** Illustration of compaction and cemention in sandstone (Slatt, 2013)

### 2.1.2 Permeability

Permeability can be defined as the flow ability of a reservoir rock through its interconnected pores. According to Tiab and Donaldson (2015); Torsæter and Abtahi (2003), the permeability of a rock depends on varies magnitude and attributes such as grain size, grain sorting, grain packing as well as cementation and compaction. They further discussed that the type of clay between the grains have the tendency to block pore space and the oil recovery may be influence by such heterogeneity.

#### Darcy's Law

Darcy developed a standard mathematical equation for the fluid flow used by most petroleum engineers. Darcy equation was used to measure the fluid flow in core plug as shown in **Fig. 2.4** and the equation can be expressed as:

$$k(Permeability[darcy]) = \frac{Q\mu L}{A(P_1 - P_2)} \tag{2.1}$$

where

| | | |
|---|---|---|
| $Q_{atm}$ | = | Flow rate $[cm^3/sec = mL/sec]$ |
| A | = | Cross-sectional area of the core sample $[cm^2]$ |
| $\mu$ | = | Viscosity of the fluid [cP] |
| $P_1$ | = | Inlet pressure [atm] |
| $P_2$ | = | Outlet pressure [atm] |
| $(P_1 - P_2)$ | = | Differential pressure across the core [atm] |

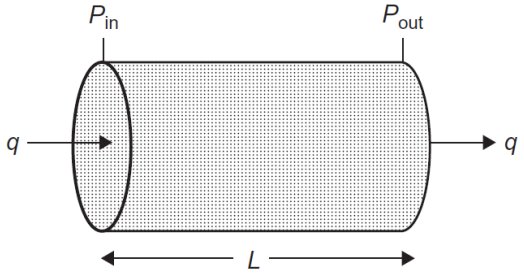


**Figure 2.4:** Darcy permeability measurement in core plug (Tiab and Donaldson, 2015).

### Absolute permeability

Permeability of clean and dry core samples of measured dimensions A and L are determined using gas as flowing fluid. This permeability can be determined in the laboratory using the Constant head permeameter. The Constant head permeameter comprises mounting the plug sample in a core holder and flowing gas through the sample at a constant rate. Pressure drop and mean gas pressure is measured and permeability calculated using **Eqn.2.1**. According to Tiab and Donaldson (2015); Torsæter and Abtahi (2003), dry gas (usually air) is used as the standard flowing fluid during the test in permeability determination. This is because it minimizes fluid-rock reaction, less alteration on the minerals in the rock and steady state is obtained. However, **Eqn.2.1** can be used for non-compressible fluid like liquid. **Eqn.2.2** as shown below would be valid to calculate permeability using dry gas.

$$k_{absolute} = \frac{2Q\mu L}{A(P_1^2 - P_2^2)} \tag{2.2}$$

### Klinkenberg Effect

Air Permeability values obtained are higher than the actual reservoir permeability. This is due to the slippage effect (Klinkenberg effect) of the dry gas that was used during the test in the laboratory. This is because dry air (gas) at low pressure will not behave as an ideal liquid.

Measured data gas permeability is therefore corrected to "equivalent liquid permeability". This correction is done to correct for the gas slippage along the pore walls. The correction is is formed by determining the gas permeability (Kg) at several different mean gas pressure (1/Pm) in the plug sample and extrapolating to find the permeability value at infinite mean gas pressure (1/Pm = 0) as shown in **Fig. 2.5**. This point becomes the equivalent liquid permeability (Kl).

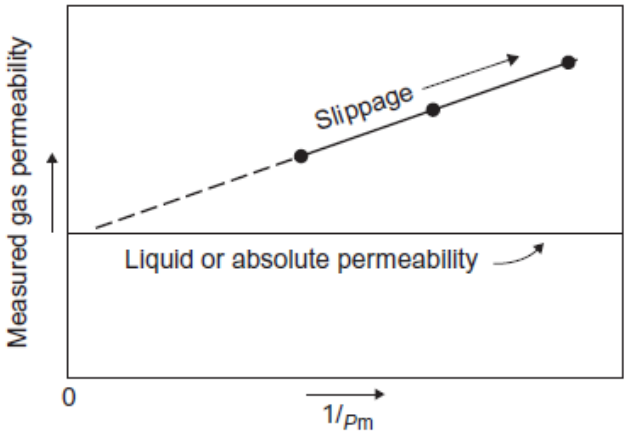


**Figure 2.5:** Klinkenberg effect (Tiab and Donaldson, 2015).

The relationship between the the measured dry air permeability and the true liquid permeability can be expressed as:

$$k_g = k_l\left(1 + \frac{b}{P_m}\right) \tag{2.3}$$

where

b = pore geometry factor

$P_m$ = mean pressure, $(P_1 - P_2)/2$

$k_g$ = gas permeability

$k_g$ = liquid permeability

According to Tiab and Donaldson (2015), the pore geometry, b can be expressed as

$$b = 6.9k_l^{-0.36} \tag{2.4}$$

### 2.1.3 Wettability and Contact Angle

**Wettability** can be defined as the tendency or the ability of one of the immiscible fluids to adhere to the surface of a solid surface in a porous medium. In a porous medium, there can be two or more more immiscible fluids. When the fluid is brought into contact with the solid surface, the liquid can spread over the solid surface or form small drops.

The **contact angle**,$\theta$, can be defined as the angle the fluid-fluid interface makes with a solid. Torsæter and Abtahi (2003), discussed that the degree of wetting or wetting condition of a solid by fluid can be determined using the contact angle and interfacial tension as shown in **Fig. 2.6**. Yuan and Lee (2013) also concluded that the measured contact angle which will eventually yield the solid surface tension, and it quantifies the wetting characteristics of a solid material.

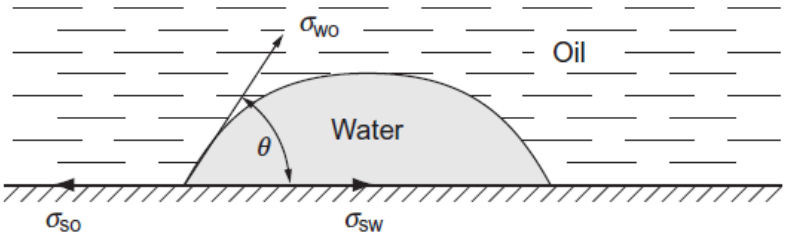


**Figure 2.6:** Contact angle and Interfacial tensions for water-oil-solid system at equilibrium expressed by Young's equation (Tiab and Donaldson, 2015).

The contact angle is measured Young's equation as shown below:

$$Cos\theta = \frac{(\sigma_{so} - \sigma_{sw})}{\sigma_{wo}} \tag{2.5}$$

where:

$\sigma_{so}$ = interfacial tension between solid and oil

$\sigma_{sw}$ = interfacial tension between solid and water

$\sigma_{wo}$ = interfacial tension between water and oil

$\theta$ = contact angle

**Adhesion tension**, $\tau$, is defined as the difference between the solid–oil and solid–water interfacial tensions and determines the favourable fluid to wet the solid. $\tau$ can be expressed in the form as shown in **Eqn.2.6**

$$Adhesiontension(\tau) = \sigma_{so} - \sigma_{sw} = \sigma_{wo}cos\theta \tag{2.6}$$

Three wetting conditions can be deduce from the adhesive tension equation.

1. The system is considered as water wet when the adhesion tension is positive , meaning the contact angle ($\theta < 90°$) and Cos$\theta$ = +.

2. When an adhesion tension is zero, indicate a neutrally wet system with contact angle ($\theta = 90°$) and and Cos$\theta$ = 0.

3. A completely oil wet system will indicate an adhesive tension of negative with its contact angle ($\theta > 90°$) and Cos$\theta$ = -.

### Wettability Evaluation

Wettability has a tremendous interest in the oil and gas recovery. The contact angle is a good technique to measure the wettability as well as the Amott cell method. However, the contact angle used gives the measurement of wettability for a mineral while the Amott cell give a quantitative representative of the rock sample based on the amount of fluids imbibe by the rock sample (Tiab and Donaldson, 2015). Since a rock comprises different minerals, it would be accurate to measure the average wettability of the rock to give a true wettability measurement for oil recovery purposes. The three types of wetting system is shown in **Fig. 2.7**

### Amott Cell Method

Using the Amott Cell Method, it practically involves four main stages or step. Amott (1959) states that the Amott cell test for wettability is based on spontaneous imbibition and forced imbibition of water and oil from the core plugs. After which the volumes of the various

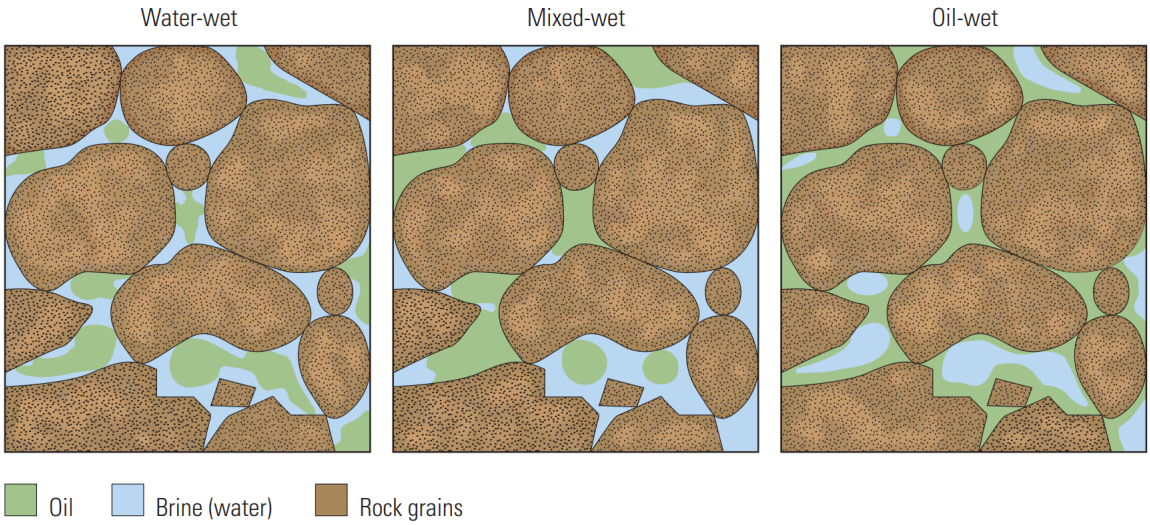


**Figure 2.7:** Various wetting systems (Abdallah et al., 1986)

fluids recorded from the various stages are used in the calculation of wettability index (WI) to determine the wetting conditions of the various samples.

The four main stages in the Amott test are as follows;

1. **Spontaneous imbibition**: process where oil saturated sample is placed in an Amott cell surrounded by water. Water imbibes in the core sample to produce oil as a function of time.

2. **Forced imbibition**: the core plugs placed in a centrifuge to force the residual oil out of the sample by water displacement.

3. **Spontaneous secondary drainage**: the water saturated core placed in an Amott cell surrounded by oil. Production of water as oil imbibes in the core sample as a function of time.

4. **Forced secondary drainage**: core samples are centrifuged in oil. The water production recorded as oil displacement forces the remaining water out.

In summary, core plugs are saturated with oil are placed in an imbibition Amott cell and surrounded by brine. The brine is allowed to imbibe the core sample displacing oil until equilibrium is reached. The volume of water ($V_{o1}$) that was able to imbibe the core is recorded. Using a centrifuge or a pump in a sealed core holder, the remaining oil is forced out

to residual oil saturation by displacing with water. The volume of oil displaced is recorded as ($V_{o2}$). The saturated core with water is then placed in an imbibition Amott cell and surrounded by oil. The oil is then allowed to imbibe the core sample displacing water until equilibrium is reached. The volume of water ($V_{w1}$) displaced is recorded. The remaining water is forced out by displacement by oil in a centrifuge and the volume of water displaced is recorded as ($V_{w2}$).

The Wettability Index (WI) is calculated using the following equation:

$$WI = \frac{V_{o1}}{V_{o1} + V_{o2}} - \frac{V_{w1}}{V_{w1} + V_{w2}} = r_o - r_w \tag{2.7}$$

where:

$r_o$= displacement by water ratio

$r_w$= displacement by oil ratio

A strongly water wet core sample will have a positive value approaching one for displacement of water and zero displacement by oil ratio. A neutrally wet sample shows nearly zero values for both displacement by water and oil ratios. Whereas, a strongly oil wet core will have a positive value approaching one for displacement by oil and a a zero value for displacement of water (Amott, 1959).

## 2.2 Mineralogy

Sedimentary rocks are formed from loosely consolidated sediments that has accumulated with time. Most sediments thus sandstones and shale on the earth surface are derived from weathering of preexisting rock fragments of various mineral types (Slatt, 2013). The commonest minerals in sedimentary are briefly described as well as their optical properties by Nichols (2009) in a table as shown in **Fig. 2.8**. According to Earle (2018), vast majority of the minerals that are formed on the Earth's crust are silicate minerals. These minerals include quartz, feldspar, mica, olivine, amphibole and clay minerals. Minerals in general are classified based on their chemical properties (chemical composition) and physical properties (structures).

| Mineral | Colour | Cleavage | Relief | Birefringence | Extinction | Other features |
|---|---|---|---|---|---|---|
| quartz | colourless | none | very low | weak | straight | unaltered |
| orthoclase | colourless | two at 90° | low | weak | slightly oblique | simple twins, often altered |
| microcline | colourless | two at 90° | low | weak | slightly oblique | cross-hatch twins, often altered |
| plagioclase | colourless | two at 93° | low | weak | oblique | lamellar twins, often altered |
| muscovite | colourless | perfect basal | moderate | strong | straight | flakes |
| biotite | brown or green | perfect basal | moderate | strong | straight | strongly pleochroic green-brown |
| hornblende | brown or green | two at 124° | moderate to high | moderate to strong | oblique up to 25° | pleochroic green-brown |
| glauconite | green | none | moderate | masked by mineral colour | straight | pleochroic green-yellow |
| calcite | colourless | two at 75° | high | very strong | symmetrical | often biogenic origin |
| dolomite | colourless | two at 75° | high | very strong | symmetrical | forms euhedral crystals |

**Figure 2.8:** Table showing the optical properties of the minerals most commonly found in sedimentary rocks (Nichols, 2009).

### 2.2.1 Common Rock-forming Silicate Minerals and Their Characteristics

According to Haldar (2013), there are about 4000 different types of minerals, but only few are relatively abundant in the composition rocks in the earth. The silicate mineral are the most abundant on the earth, accounting for 90% of the earth's crust. They contain silicon and oxygen and have a fundamental building block, thus silicon-oxygen tetrahedron.

#### Quartz

Quart is the most common mineral and abundant in most sediments of rocks. Quartz can easily be distinguished from other mineral in thin section because they are usually unaltered, have irregular grains and may lack visible twinning or cleavage (MacKenzie and Guilford, 2014). Under plane-polarized light, it shows colourless or clear colour with no cleavage and low relief. Under crossed-polarised light, it displays a low or white interference colours (**Fig. 2.9**) and will display a yellowish interference when the thin section is thicker than the standardize thickness of 30 micrometer ($\mu$m).

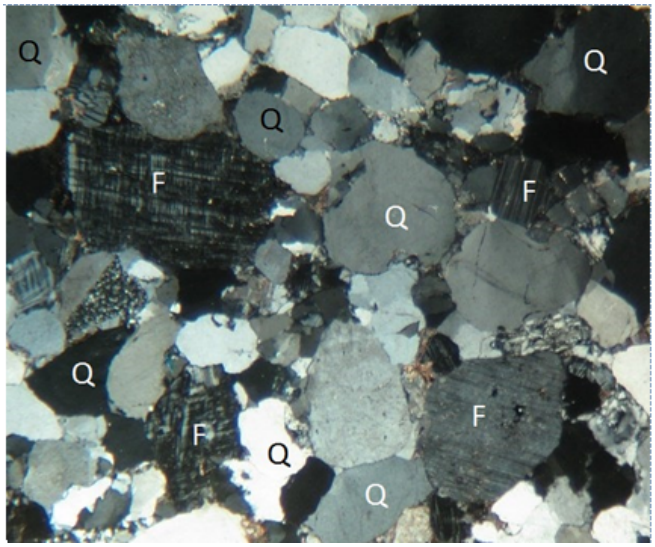


**Figure 2.9:** Thin section of arkosic sandstone under crossed-polarized light: Q=quartz, F=feldspar (Earle, 2018).

### Feldspar

According to Dyar et al. (2008), although quartz are the most abundant mineral species in the earth's crust, feldspar happens to be the most abundant group. There are three most common forms of feldspar minerals are orthoclase, (K-feldspar) and two types of plagioclase feldspar: albite (sodium only) and anorthite (calcium only) as shown in **Fig. 2.10**. Potassium feldspar also known as alkali feldspar is more abundant than plagioclase on earth. Feldspar can be distinguished by from other mineral by the distinctive twinning in crossed polarized light and cleavage in plane polarized light. Potassium feldspar displays carlsbad twinning under crossed polarized light, whereas plagioclase displays albite twinning as shown in **Fig. 2.11(a) & 2.11(b)** respectively.

### Mica

According to Adams et al. (2017), mica form minor constituent in most sandstones. There are various types of mica, but two forms of mica are frequently encountered; white mica (muscovite) and the brown mica (biotite). However, muscovite is more common than biotite because of its resistant to weathering. Biotite in sediment are easily altered to chlorites and clays.

Muscovite is colourless under plane polarized light, flakes with 1 perfect cleavage. Bi-

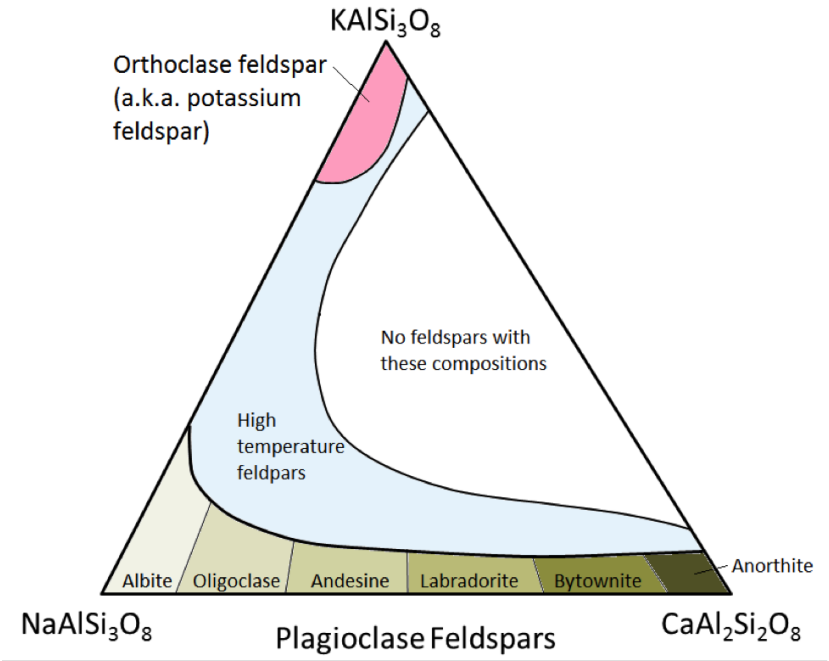


**Figure 2.10:** Composition of feldspar minerals (Earle, 2018).

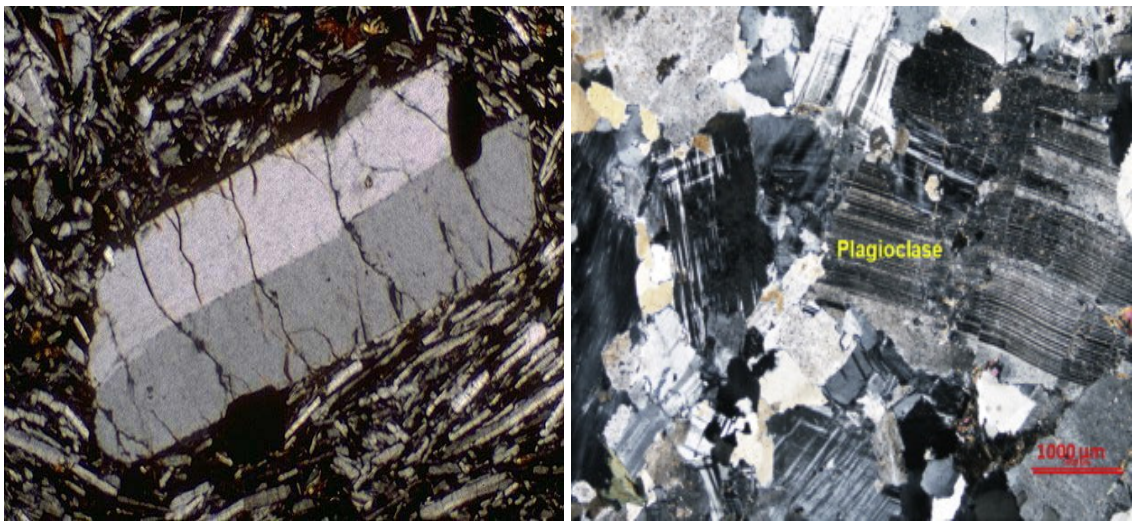


(a) K-feldspar showing carlsbad twinning (b) Plagioclase showing albite twinning

**Figure 2.11:** The twinning types displayed in feldspar under crossed polarized light, (Haldar, 2013).

otite displays pale to deep greenish brown, or brown under plane polarized light. It exhibit perfect mica cleavage in most sections and little or moderate pleochroism. Biotite has a high birefringence which can be partly masked by deep intrinsic colour, very striking under cross-polars.

Muscovite and biotite under thin section as shown in **Fig. 2.12**

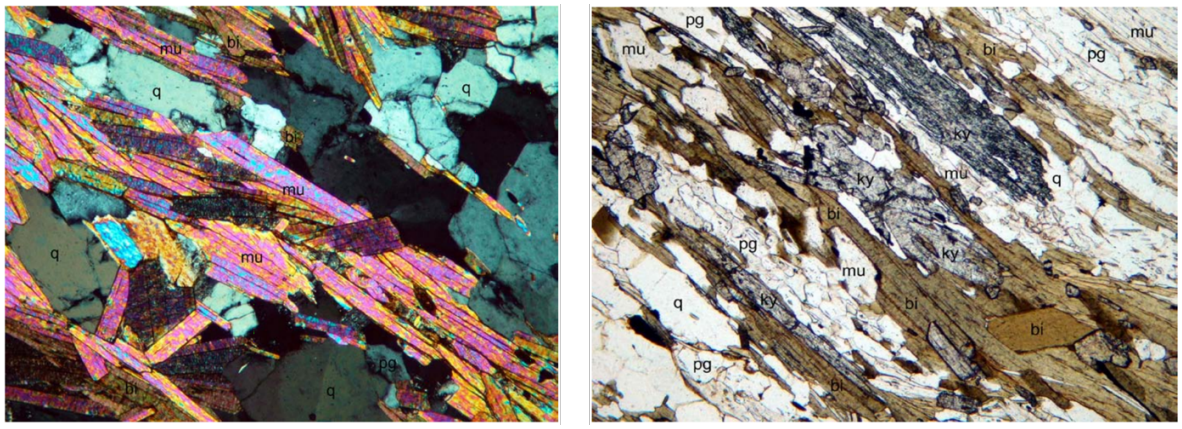


**Figure 2.12:** Thin section of muscovite and biotite under crossed-polarized and plane-polarized light respectively: mu=muscovite, bi=biotite, q=quartz, pg=plagioclase (Charles and Merguerian, 2014).

Chapter 3

# Data set and Methodology

There are several approach in determining porosity, permeability and wettability as well as the factors/conditions that control these rock properties. For this project, the following are the main approaches/methods.

1. Core analysis.

2. Petrographic analysis using Optical Microscope and Scanning Electron Microscope (SEM) analysis.

A standard core analysis program normally consists of plug cleaning and drying and determination of porosity, gas Permeability, wettability of the sample and grain density. Evaluation of porosity, permeability, lithology and texture as well as wettability is information derived from routine/conventional and special core analysis. Porosity is calculated using Helium Porosimeter, permeability is measured from Constant Head Permeameter and combined Amott test was used for the wettability investigation.

The identification of minerals in the rock samples were done by observing images of thin sections viewed under a polarizing microscope. By studying the samples under SEM, detailed information about the unknown samples was obtained. SEM can be useful in the identification of grain coatings, mineral associations as well as quartz overgrowth (Niazia et al., 2019). Backscattered electron images (BEI) in combination with Energy Dispersive Spectrometer (EDS) were used to calculate the elemental composition and identification of the minerals.

## 3.1 Data set

### 3.1.1 Sample size and measurement

Typically, the sizes of core plug for analysis comes in various dimensions. For this study, four core plugs were used for the analysis. The core plugs are made up of three sandstone outcrops and one core plug of Berea sandstone. The core plugs measure about 3.7cm in diameter by 3.1 to 4.1cm long.

### 3.1.2 Thin sections of the sample

Blue epoxied thin sections of the four core plugs were available for the SEM analysis as well as the microscopic analysis.

## 3.2 Methodology

### 3.2.1 Core Analysis Preparation

Core plugs might contain some residue fluids in addition to the rock matrix. This residue fluids may interfere with the analysis measurements at the laboratory. The core plug samples must be thoroughly cleaned to completely remove the fluid in the pore spaces and dried prior to analysis (Torsæter and Abtahi, 2003). As stated by (Gant et al., 1988), there are two main reasons why core is cleaned. Core is cleaned to remove all fluid to for the measurement of porosity, permeability and fluid saturation. The other reason is to restore the altered wettability of a core.

#### Cleaning Method

There are various types of methods for the core cleaning prior to porosity and permeability measurements. These methods include the Direct Injection of Solvent, centrifuge flushing, gas driven solvent extraction, Soxhlet extraction, Dean-Stark distillation-extraction and Vacuum distillation (Torsæter and Abtahi, 2003).

**Soxhlet Extraction**

In this study, the method used in the cleaning was the Soxhlet Extraction (**Fig. 3.1**). This is the most common method used for cleaning samples in the laboratory for porosity and permeability measurements. The standard solvents used in Soxhlet extraction apparatus for cleaning are toluene and methanol. However, methanol was used for the cleaning in this study.

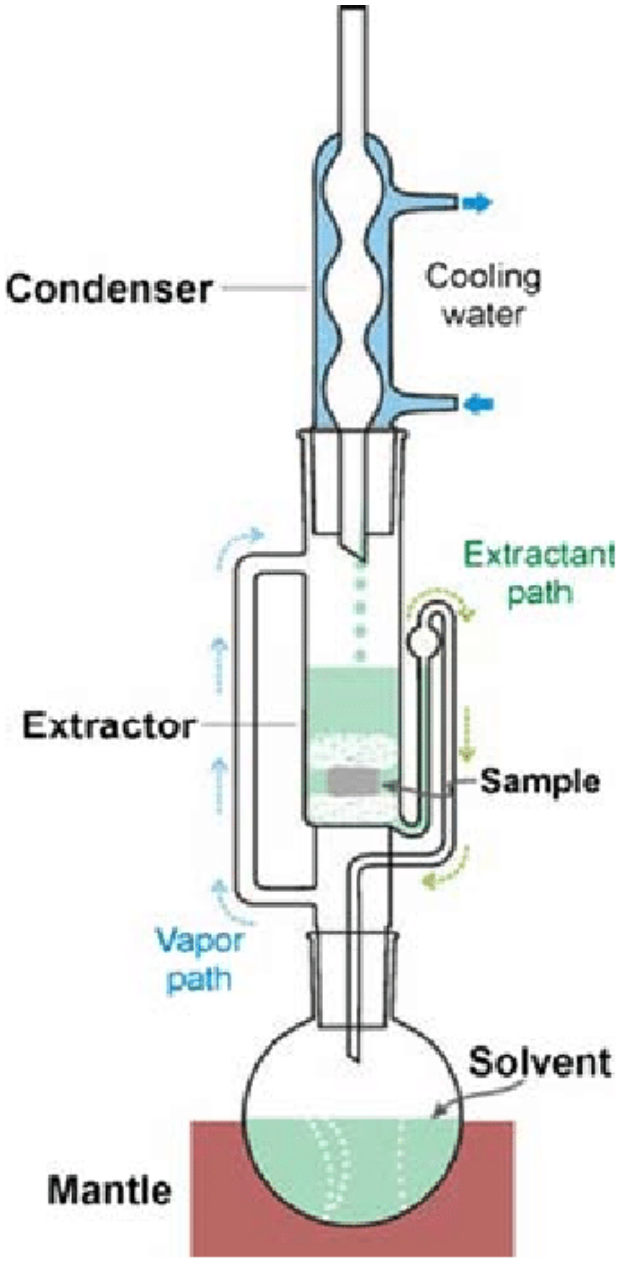


**Figure 3.1:** Soxhlet extraction apparatus (Dabbs et al., 2006).

As shown in **Fig. 3.1**, the sample is soaked in the solvent in the flask mounted over a heating mantle. This is a distillation process which cleans the core samples. Methanol in the Pyrex flask is gently heated until its vapour rises from flask and the core gets immersed in the methanol vapors (at approximately 110°C) (Torsæter and Abtahi, 2003). The water in the core sample gets vaporised. The methanol and the water vapour cools down upon reaching the inner chamber of the condenser, the cold water then circulates about in the inner chamber condenses both vapors to immiscible liquids. The core sample get soaked with the dripping water from the base of the condenser and dissolves any available fluid in the core sample in the extractor. The solvent siphoned off into the boiling flask through the extractant path. Another cycle begin again until the core is completely cleaned. This process require several days for a complete extraction.

Gant et al. (1988) simplified the process of the Soxhlet apparatus as "core sample soaked in a hot solvent, which is regularly siphoned off, then distilled, condensed, and distributed back to the extractors".

#### Drying

After the core sample have been thoroughly cleaned, it is then dried in hot oven (60 - 105°C). The purpose of drying is to remove connate water or solvents left in the pores during the cleaning process. Precaution might be exercised during this procedure since clay structures may be altered in samples that contain some amount of clay minerals. Therefore drying the sample at 60°C and 40 % relative humidity might have less impact on the sample (Torsæter and Abtahi, 2003).

### 3.2.2 Experiments From Core Analysis

1. **Porosity**

   Porosity is the volume of the rock matrix which is fluid filled (oil, water, gas), which is expressed as the percentage or fraction of the of the bulk rock volume. However, effective porosity which is the sum of all the interconnected pore space is calculated during core analysis. Effective porosity can be calculated based on 2 or 3 of the parameters: bulk volume, grain volume, pore volume and grain density. According to (Torsæter

and Abtahi, 2003), bulk volume can be computed using measured dimensions of a uniformly shaped sample, pore volume determined from the helium porosimeter method (**Fig. 3.2**) and grain volume determined from Boyle's law which is often employed with helium(gas).

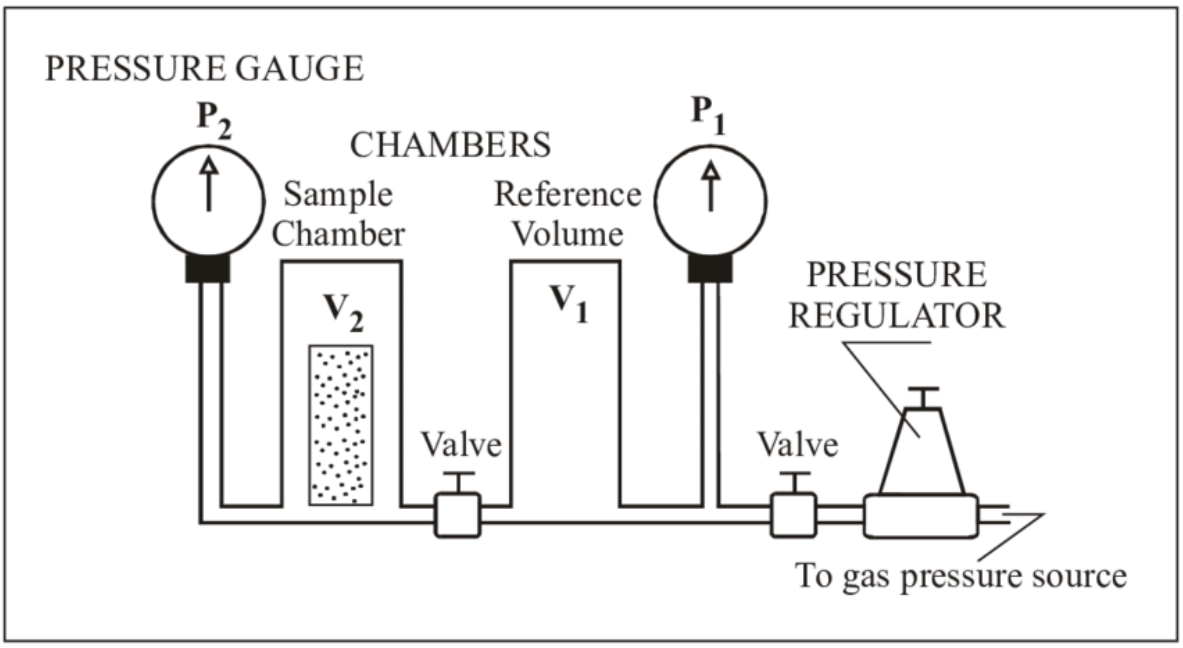


**Figure 3.2:** Schematic diagram of helium porosimeter apparatus (Torsæter and Abtahi, 2003).

**Helium Porosimeter Method**

Pore volume measurement was done in the laboratory as shown in **Fig. 3.3** using the Helium Porosimeter Method where the dry core samples were resaturated with gas (helium). This method uses the principle of gas expansion which is known as the Boyle's law method, because of the inert state of helium, it is not easily absorbed onto the surface of the minerals in the sample (Cone and Kersey, 1992; Torsæter and Abtahi, 2003).

**Procedure:**

(a) The dimensions (length and diameter) of the dried core samples are measured using a caliper to be able to calculate the bulk volume as shown in Equation 4.1 and 4.2.

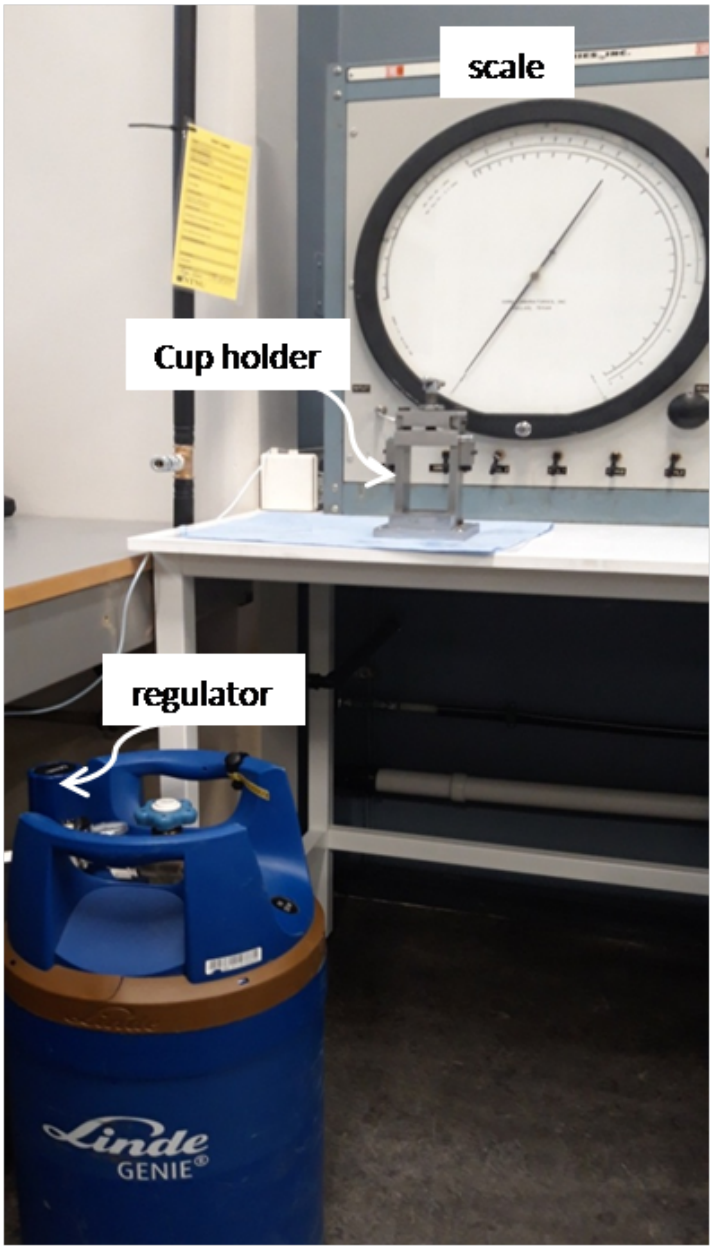


**Figure 3.3:** Setup of helium porosimeter apparatus in the laboratory.

(b) The regulator as shown in **Fig. 3.3** was regulated to 10 bar to supply helium to the porosimeter.

(c) The volume of matrix cup with core was determined.

(d) The volume of matrix cup without core was determined.

**Vacuum saturation/liquid saturation Method**

This method/technique was used for measuring pore volume of core sample from the difference in the weight of saturated core and the dry core.

**Procedure:**

(a) Weigh the dry core samples ($W_{dry}$).

(b) Cores were put in a vacuum saturation device (**Fig. 3.4**) and allow vacuum pump to run for an hour.

(c) All of the air are displaced and core saturated with 3%wt NaCl saltwater/brine, with density 1.03g/$cm^3$.

(d) Weigh the saturated core ($W_{wet}$).

(e) Calculate the weight of brine ($W_{brine}$) = $W_{wet}$ - $W_{dry}$.

(f) Calculate pore volume (Vp) = $W_{brine}/\rho_{brine}$.

(g) Calculate effective porosity (Equation 4.5).

**Figure 3.4:** Setup of vacuum device in the laboratory.

2. **Permeability**

Permeability is the the flow capacity of a rock matrix/formation. Various techniques are used in the laboratory to measure the absolute permeability of a core sample. In this study, the constant head permeameter as shown in **Fig. 3.5** was used to measure the permeability.

### Constant Head Permeameter

Permeability was measured by passing gas through the dried and clean core sample and measuring the flow rate and pressure drop.

**Fig. 3.6** shows the schematic diagram of the constant head permeameter where air is used as gas. Hassler core holder was used for an excellent tightness and different sample sizes.

According to Torsæter and Abtahi (2003), "Upstream and downstream pressures are measured by manometers on both sides of the core and air flow is measured by means of a calibrated outlet". Air permeability calculated using **Eqn.3.1**, where the flow rate (Q) is measured at atmospheric condition ($P_{atm}$=1).

$$Q_{atm} = \frac{Ak}{\mu L} \times \frac{(P_1^2 - P_2^2)}{2P_{atm}} \tag{3.1}$$

where:

| | | |
|---|---|---|
| A | = | Cross-sectional area of the core sample [$cm^2$] |
| D | = | Diameter of core sample [cm] |
| k | = | Permeability [darcy] |
| L | = | Length of core sample [cm] |
| $Q_{atm}$ | = | Flow rate [$cm^3/sec = mL/sec$] |
| $\mu$ | = | Viscosity of the flowing liquid [cP] |
| $(P_1^2 - P_2^2)$ | = | Differential pressure across the core [atm] |
| $P_{atm}$ | = | Atmospheric pressure [atm] |

The permeability k is then plotted against 1/the mean pressure ($P_m$)[atm].

The absolute permeability of liquid for air permeability experiment is calculated using the Klinkenberg effect.

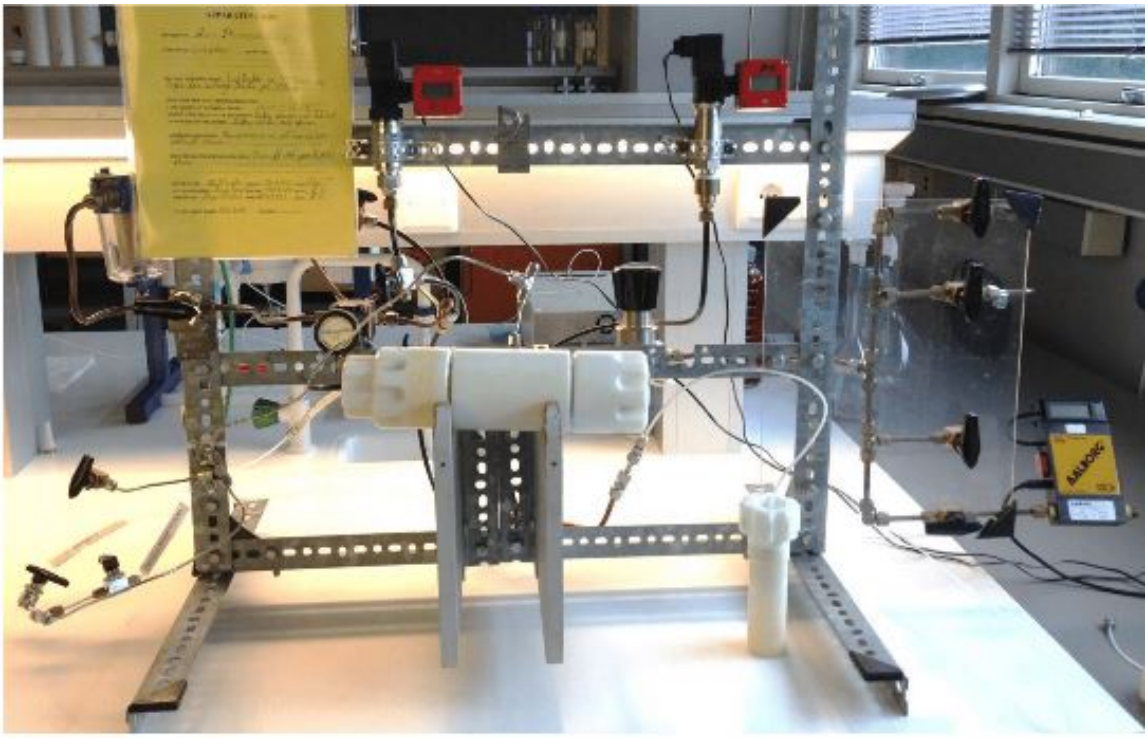

**Figure 3.5:** Setup of constant head permeameter in the laboratory.

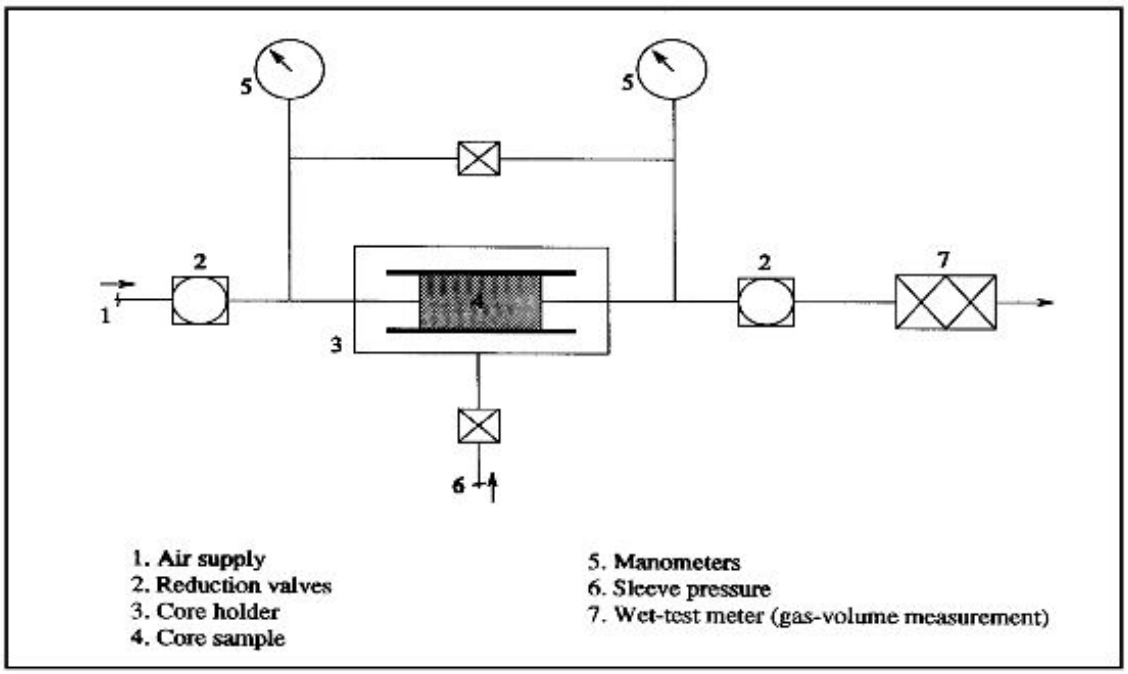


**Figure 3.6:** Schematic diagram of constant head permeameter.

3. **Wettability**

   The preference of a fluid to adhere to the surface of a material in the presence of another fluid is determined by its wettability. Wettability is also the fundamental and important property that controls the fluid distribution within the pore of a rock.
   There are three main methods to measure the wettability of the rock; sessile drop method (contact angle), Amott cell method and the USBM (U.S Bureau of Mines) method. However in this study, the amott method was used for the wettability experiment.

   **Amott Cell Method**

   This method is the most common and widely accepted method to determine wettability in the oil and gas industry.
   In this method, the core sample is saturated with oil and placed in Amott ambibition cell filled with 3 wt% NaCl brine (**Fig. 3.7a**). The brine is allowed to imbibe into the core sample for some days. The volume of oil displaced is then measured and recorded. The core is removed from the cell and flooded with water using centrifuge. The volume of oil displaced after the remaining oil in the core is forced down by residual saturation is measured and recorded.

   The core, which is now saturated with water is now placed in Amott cell filled with oil (**Fig. 3.7b**). The oil imbibes the core displacing the water. The volume of water displaced is measured and recorded. The remaining water in the core is forced out in a centrifuge by displacement. The volume of water displaced is then recorded.

   After all the volumes recorded, the wettability index (WI) was then calculated. The wettability index ranges from -1 to +1, where

   WI=1, completely water wet
   WI=0, neutral
   WI=-1, completely oil wet.

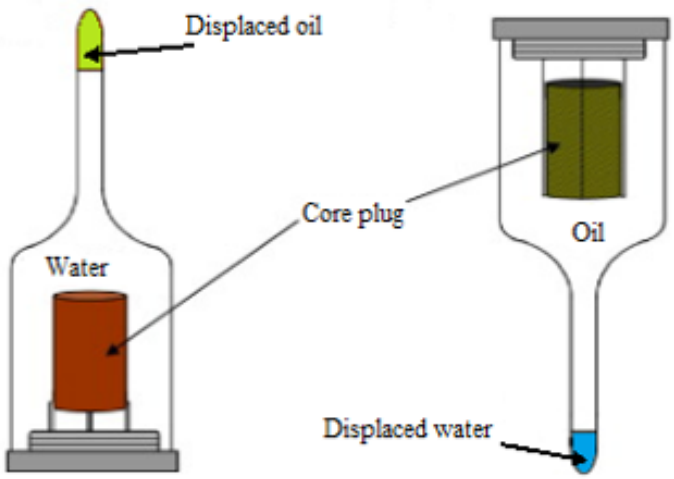


**Figure 3.7:** (a)Amott imbibition cell with oil saturated core and (b)Amott imbibition cell with water saturated core.

### 3.2.3 Petrography Analysis

Minerals in the samples were identified and analysed by Optical inspection using the polarized light microscope and scanning electron microscope (SEM). The Backscattered Electron Images and Energy Dispersive Spectra were used in conjunction with each other.

#### Thin Section Analysis

The thin sections were examined under a polarized light microscope (**Fig.** 3.8), which allowed specimen to be viewed both under plane-polarized and cross-polarized light. The polarized light microscope aided in the identification and detailed studies of minerals.

The common minerals observed in the thin sections were mainly quartz, feldspar, mica, kaolinite and some accessory minerals. When light is being transmitted through a mineral, it produces its own distinctive effect on the light. However according to West (1985), minerals can be identified based on their mineral characteristic shapes and cleavage when examined under plan-polarised light.

#### SEM

In this study, a scanning electron microscope was used to provide useful information about the composition and to identify minerals in a rock sample. In a scanning electron microscope, the sample is irradiated by a high energetic electron beam, causing it to send out different signals. Backscattered electron images (BEI) is used for studying mineral zoning and textural relations. This method is based on the differences in intensity of minerals reflecting their atomic number, where heavy minerals appear less dark than lighter minerals.

According to Kandarpa et al. (1981), rock samples with low atomic number elements, there is few scattering near the surface thereby the electron beams are been absorbed and few incoming electrons backscattered. Those with high atomic number elements has large proportion of the incoming electrons are backscattered. Therefore, the higher the atomic number, the higher the fraction of electrons that are been backscattered.

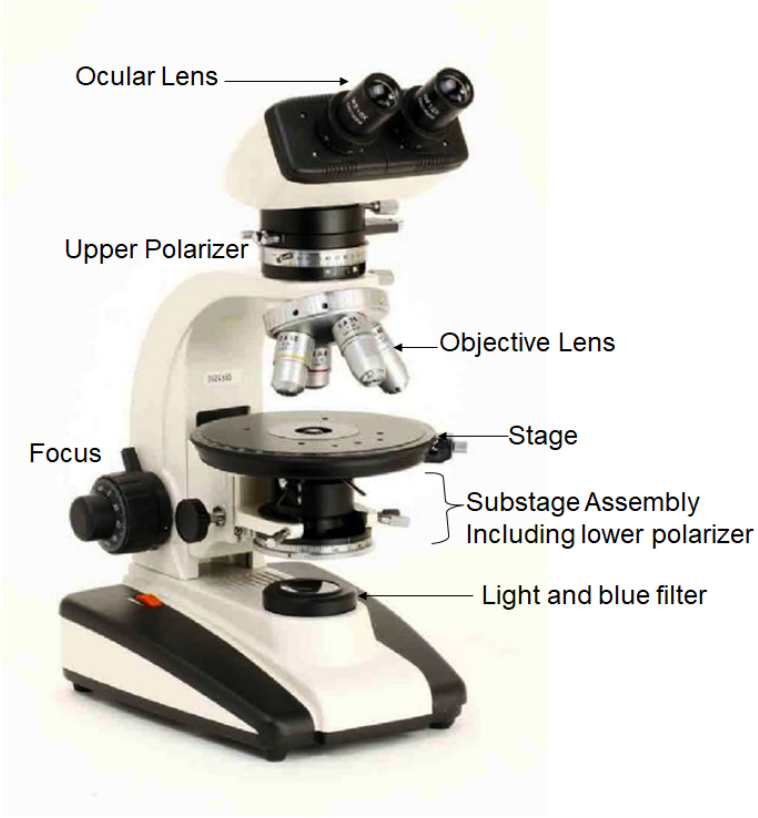


**Figure 3.8:** Polarized Light Microscope Configuration, courtesy `http://geologyscience.com/general-geology/optical-properties-of-minerals/`, september 2019.

### EDS-Analysis

Energy dispersive spectra, can be very useful to calculate the element proportions and the mineral formulas in an unknown sample. After doing a EDS analysis, a spectrum will appear with different peaks. The peak position reflects the energy and each element have a standard energy peak. The analysis will then give you the element types in the sample. Furthermore, the peak intensity is proportional to element concentrations. Therefore, comparison with analyses of mineral standards allows us to calculate the element proportions and mineral formulas.

The porosity appear in a black colour on the analysis. This is because porosity is the empty space between the grains and does not contain any mass. Hence, the EDS analysis will not have any energy to reflect and it appears black. The porosity in the samples was mostly intergranualar, but few intragranular porosity was also identified.

Chapter 4

# Results

Four core samples were analysed and from the core laboratory . One (1) core sample from Berea sandstone of known permeability and three (3) different sandstone samples.

Where,

| | | |
|---|---|---|
| BSS | = | Berea sandstone core sample |
| Core sample 1-3 | = | various sandstone samples |

## 4.1 Porosity

There are different methods for estimating the porosity of a core sample. However in this experiment, the helium porosimeter method and the saturation method was used in the calculation.

### 4.1.1 Helium Porosimeter Method

The Helium porosity parameters obtained from the experiment in the laboratory: length of core sample (L), diameter of the core sample (D), Volume of matrix cup without core ($V_1$), Volume of matrix cup with core ($V_2$), grain volume (Vg) as well as estimated bulk volume (Vb) and pore volume (Vp).

The bulk volume was calculated using the radius (r) of the core sample and the length of core as shown in the equation below.

$$\text{Bulk volume (Vb)} = \pi r^2 \times L \tag{4.1}$$

Or the diameter (D) can be used directly in calculating the bulk volume with the following formula.

$$\text{Bulk volume (Vb)} = \pi \frac{D^2}{4} \times L \tag{4.2}$$

Grain volume estimated from the difference in volume of matrix cup without core $V_1$ and volume of matrix cup with core $V_2$.

$$\text{Grain volume (Vg)} = V_1 - V_2 \tag{4.3}$$

Pore volume estimated from the difference in bulk volume (Vb) and grain volume (Vg).

$$\text{Pore volume (Vp)} = Vb - Vg \tag{4.4}$$

Effective porosity ($\phi_e$) calculated as a ratio of pore volume to the bulk volume as shown in the following equation.

$$\phi_e = \frac{Vp}{Vb} \times 100 \tag{4.5}$$

**Table 4.1:** Helium Porosity Parameters.

| **Sample No.** | **D** cm | **L** cm | **Vb** $cm^3$ | **V1** $cm^3$ | **V2** $cm^3$ | **Vg** $cm^3$ | **Vp** $cm^3$ | $\phi_e$ % |
|---|---|---|---|---|---|---|---|---|
| BSS | 3.75 | 4.14 | 45.72 | 62 | 26.00 | 36.00 | 9.72 | 21 |
| 1 | 3.75 | 3.75 | 41.42 | 62 | 30.40 | 31.60 | 9.82 | 24 |
| 2 | 3.74 | 3.73 | 40.98 | 62 | 32.00 | 30.00 | 10.98 | 27 |
| 3 | 3.75 | 3.19 | 35.23 | 62 | 33.60 | 28.40 | 6.83 | 19 |

From the porosity values as shown in **Table 4.1**, core sample 2 have the highest porosity value of 0.27 with the highest pore volume of 10.98. These porosity value are not influenced by the mineralogical composition of the sample.

### 4.1.2 Liquid Saturation Method

This method/technique, the pore volume of core sample was determined from the ratio of the difference in the weight of saturated core and the dry core to the density of brine. The density of brine used for the porosity calculation was 1.03g/$cm^3$.

The weight of brine ($W_{brine}$) was determined by the difference in the weight of saturated core ($W_{wet}$) and dry core sample ($W_{dry}$) using **Eqn.4.6**.

$$W_{brine} = W_{wet} - W_{dry} \tag{4.6}$$

The pore volume was calculated using the weight of brine ($W_{brine}$) and the density of brine ($\rho_{brine}$) as shown in (**Eqn.4.5**).

$$Vp = W_{brine}/\rho_{brine} \tag{4.7}$$

**Table 4.2:** Liquid Saturation Parameters.

| **Sample No.** | **Wet weight** g | **Dry weight** g | **Brine weight** g | **Vb** $cm^3$ | **Vp** $cm^3$ | $\phi_e$ % |
|---|---|---|---|---|---|---|
| 1 | 91.2 | 80.41 | 10.79 | 41.42 | 10.42 | 25.16 |
| 2 | 87.89 | 76.29 | 11.61 | 40.98 | 11.22 | 27.40 |
| 3 | 78.28 | 70.43 | 7.85 | 35.23 | 7.59 | 21.50 |

## 4.2 Permeability

The following are permeability results obtained from the laboratory. Air viscosity ($\mu_{air}$) of 0.0179cP was used for the calculation. Since dry gas was used for the experiment, K was calculated using the following equation as shown below.

$$k = \frac{2Q\mu L}{A(P_1^2 - P_2^2)}$$

| | | |
|---|---|---|
| A | = | Cross-sectional area of the core sample [$cm^2$] |
| D | = | Diameter of core sample [cm] |
| k | = | Permeability [darcy] |
| L | = | Length of core sample [cm] |
| $Q_{atm}$ | = | Flow rate [$cm^3/sec = mL/sec$] |
| $\mu$ | = | Viscosity of the flowing liquid [cP] |
| $(P_1^2 - P_2^2)$ | = | Differential pressure across the core [atm] |
| $P_{atm}$ | = | Atmospheric pressure [atm] |

The Klinkenberg effect correction where gas permeability is plotted against 1/Pm was used to get the absolute permeability of the core samples. From the following graphs (**Fig. 4.2, 4.4, 4.6 and 4.8**), the absolute permeability ranges between 23mD to 651mD, where core sample BSS having the highest value of 651.2mD and core sample 1 with the least value of 23.3mD. The numerical data for all the cores are given in (**Fig. 4.1, 4.3, 4.5 and 4.7**).

The chart for the various core samples and their Klinkenberg effect correction graphs are as follows:

**Calculation chart and Klinkenberg effect correction graph for core sample BSS**

| | Data recorded in lab | | | | Data for graph | | |
|---|---|---|---|---|---|---|---|
| | P1 | P2 | ΔP | Q | Q | 1 / Pavg | k |
| | [bar] | [bar] | [bar] | [l/min] | [ml/s] | [atm-1] | [mD] |
| Core Sample BSS | 1.20 | 1.00 | 0.20 | 2.05 | 34.17 | 0.92 | 1066.72 |
| | 1.40 | 1.20 | 0.20 | 2.30 | 38.33 | 0.78 | 1012.68 |
| | 1.60 | 1.40 | 0.20 | 2.50 | 41.67 | 0.68 | 953.98 |
| | 1.80 | 1.60 | 0.20 | 2.60 | 43.33 | 0.60 | 875.41 |
| | 2.00 | 1.80 | 0.20 | 2.66 | 44.33 | 0.53 | 801.34 |

| | | |
|---|---|---|
| L | 4.150 | cm |
| d | 3.760 | cm |
| A | 11.104 | $cm^2$ |
| $\mu_{air}$ | 0.0179 | cp |

| Ka [md] |
|---|
| 651.2 |

**Figure 4.1:** Chart of the data recorded in the laboratory used for the permeability calculation (Core BSS).

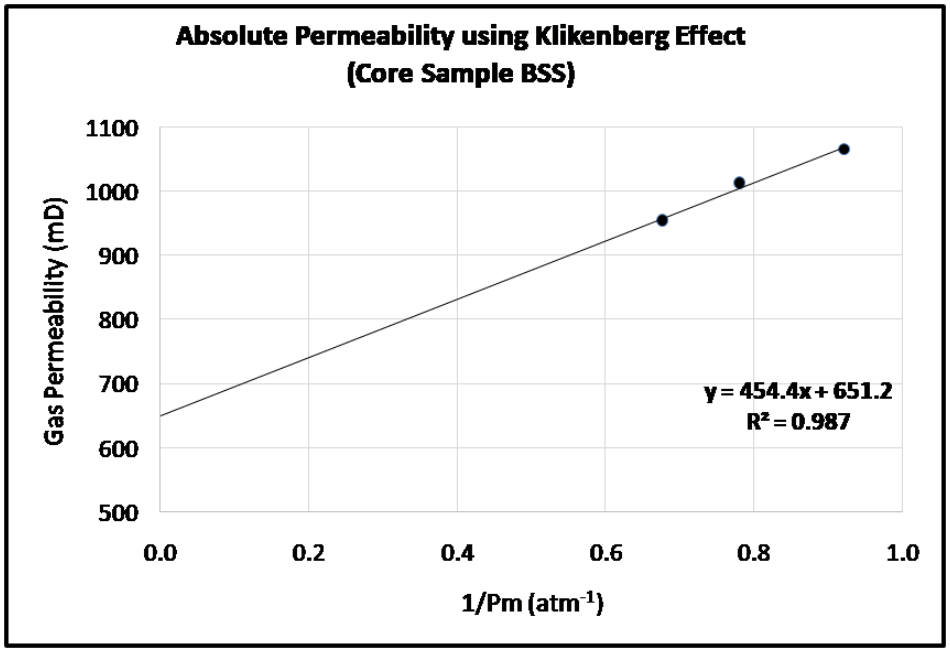


**Figure 4.2:** Klinkenberg effect correction for permeability (Core BSS).

**Calculation chart and Klinkenberg effect correction graph for core sample 1**

| | Data recorded in lab | | | | Data for graph | | |
|---|---|---|---|---|---|---|---|
| | P1 | P2 | ΔP | Q | Q | 1 / Pavg | k |
| | [bar] | [bar] | [bar] | [L/min] | [ml/s] | [atm-1] | [mD] |
| Core Sample 1 | 1.50 | 1.00 | 0.50 | 0.24 | 4.00 | 0.81 | 39.10 |
| | 2.00 | 1.50 | 0.50 | 0.31 | 5.17 | 0.58 | 36.07 |
| | 2.50 | 2.00 | 0.50 | 0.35 | 5.83 | 0.45 | 31.67 |
| | 3.00 | 2.50 | 0.50 | 0.38 | 6.33 | 0.37 | 28.14 |
| | 3.50 | 3.00 | 0.50 | 0.37 | 6.17 | 0.31 | 23.18 |

| | | |
|---|---|---|
| L | 3.750 | cm |
| d | 3.790 | cm |
| A | 11.282 | $cm^2$ |
| $\mu_{air}$ | 0.0179 | cp |

| Ka [md] |
|---|
| 23.53 |

**Figure 4.3:** Chart of the data recorded in the laboratory used for the permeability calculation (Core 1).

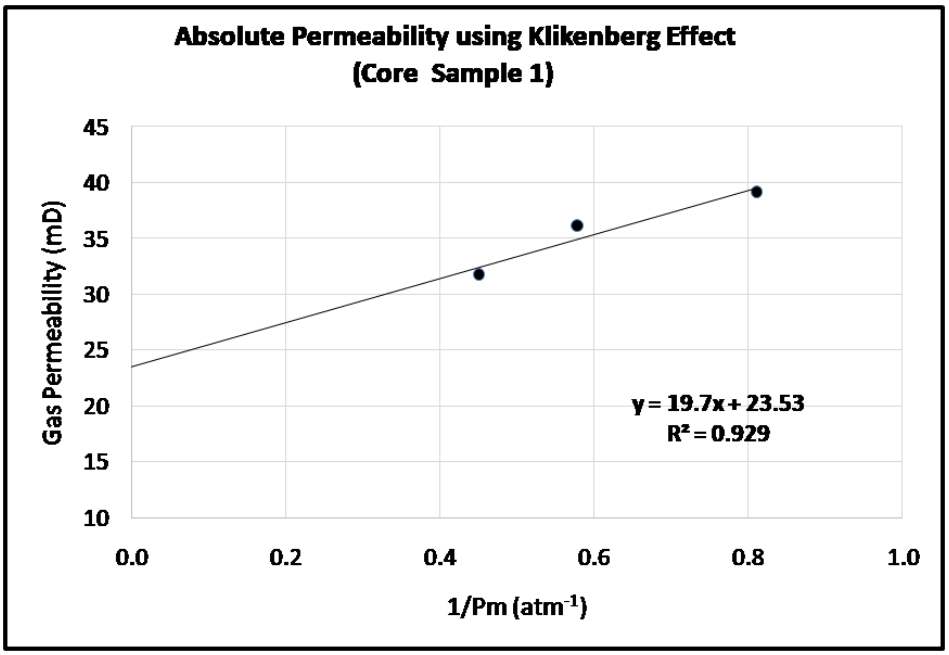


**Figure 4.4:** Klinkenberg effect correction for permeability (Core 1).

**Calculation chart and Klinkenberg effect correction graph for core sample 2**

| | Data recorded in lab | | | | Data for graph | | |
|---|---|---|---|---|---|---|---|
| | P1 | P2 | ΔP | Q | Q | 1 / Pavg | k |
| | [bar] | [bar] | [bar] | [L/min] | [ml/s] | [atm-1] | [mD] |
| Core Sample 2 | 1.20 | 1.00 | 0.20 | 1.00 | 16.67 | 0.92 | 467.69 |
| | 1.40 | 1.20 | 0.20 | 1.05 | 17.50 | 0.78 | 415.52 |
| | 1.60 | 1.40 | 0.20 | 1.11 | 18.50 | 0.68 | 380.70 |
| | 1.80 | 1.60 | 0.20 | 1.07 | 17.83 | 0.60 | 323.81 |
| | 2.00 | 1.80 | 0.20 | 1.05 | 17.50 | 0.53 | 284.31 |

| | | |
|---|---|---|
| L | 3.730 | cm |
| d | 3.760 | cm |
| A | 11.104 | $cm^2$ |
| $\mu_{air}$ | 0.0179 | cp |

| Ka [md] |
|---|
| 140.1 |

**Figure 4.5:** Chart of the data recorded in the laboratory used for the permeability calculation (Core 2).

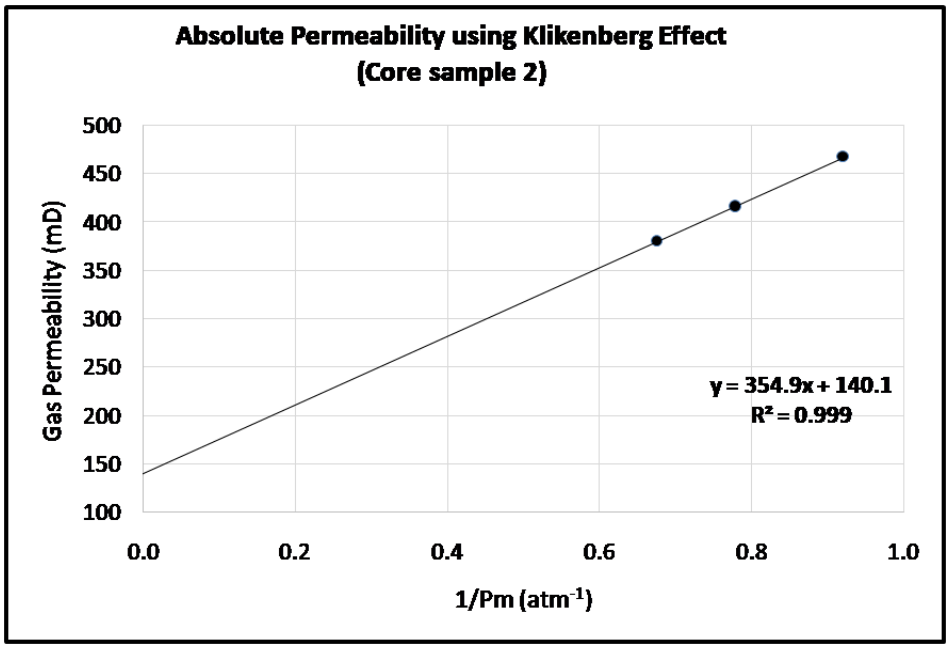


**Figure 4.6:** Klinkenberg effect correction for permeability (Core 2).

**Calculation chart and Klinkenberg effect correction graph for core sample 3**

| | Data recorded in lab | | | | Data for graph | | |
|---|---|---|---|---|---|---|---|
| | P1 | P2 | ΔP | Q | Q | 1 / Pavg | k |
| | [bar] | [bar] | [bar] | [L/min] | [ml/s] | [atm-1] | [mD] |
| Core Sample 3 | 1.20 | 1.00 | 0.20 | 0.50 | 8.33 | 0.92 | 199.99 |
| | 1.40 | 1.20 | 0.20 | 0.53 | 8.83 | 0.78 | 179.38 |
| | 1.60 | 1.40 | 0.20 | 0.58 | 9.67 | 0.68 | 170.12 |
| | 1.80 | 1.60 | 0.20 | 0.60 | 10.00 | 0.60 | 155.29 |
| | 2.00 | 1.80 | 0.20 | 0.63 | 10.50 | 0.53 | 145.89 |

| | | |
|---|---|---|
| L | 3.190 | cm |
| d | 3.760 | cm |
| A | 11.104 | $cm^2$ |
| $\mu_{air}$ | 0.0179 | cp |

| Ka [md] |
|---|
| 85.75 |

**Figure 4.7:** Chart of the data recorded in the laboratory used for the permeability calculation (Core 3).

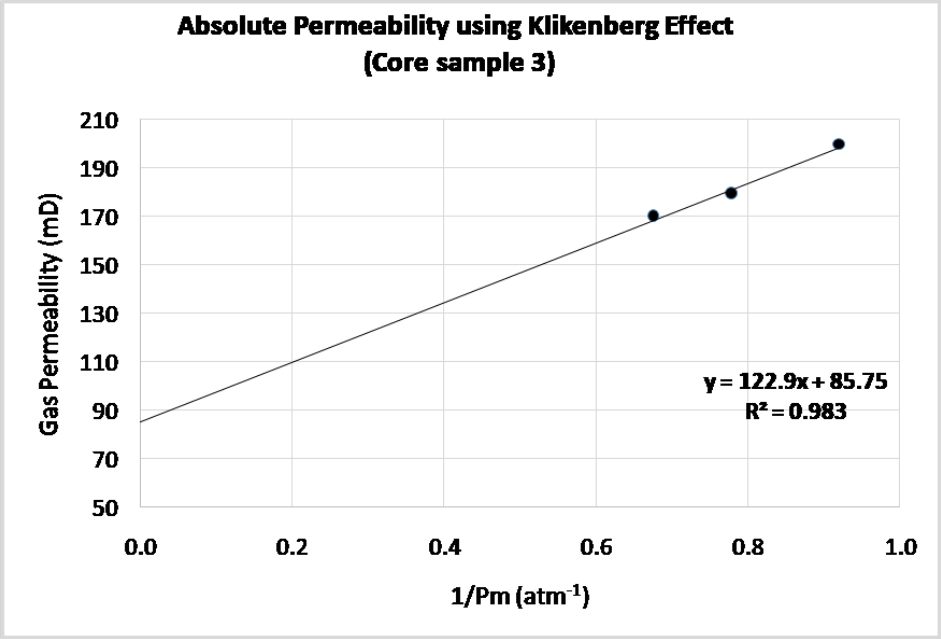


**Figure 4.8:** Klinkenberg effect correction for permeability (Core 3).

## 4.3 Wettability

The drainage (displacement) process was carried out using the Beckman centrifuge in the laboratory. However, this equipment can be used for three (3) core samples at a time. Although four (4) core samples were used for the porosity and permeability experiment, core sample 1, 2 and 3 were used for the wettability experiment since Berea sandstone is a well known sandstone sample used in the laboratory.

The experiment was first carried out by saturating the core samples with brine in a vacuum saturation device (**Fig. 3.4**) before the forced drainage (displacement by oil) performed using the Beckman centrifuge to acquire the volume of water produced ($V_{w2}$). After which the volume of oil produced was acquired ($V_{o1}$) by imbibing the core with water in an Amott cell, followed by forced imbibition (displacement by water) using the Beckman centrifuge to acquire the volume of oil ($V_{o2}$) after centrifuging. The core sample were finally placed in an Amott cell filled with oil to imbibe the water saturated core to acquire the volume of water produced ($V_{w1}$).

The volumes recorded are shown in **Table 4.3** with the wettability index for each core sample using **Eqn. 4.8**. Since none of the core samples imbibed oil, the displacement by water ratio ($r_o$) was used in calculating the WI.

From the Wettability Index chart as shown in **Table 4.4**, the three (3) core sample are all strongly water wet with core sample 1 and 2 having the highest WI value of 0.98 and core sample 3 having 0.73.

**Table 4.3:** Wettability (Amott Cell Method)

| | **Displacement by water (mL)** | | **Displacement by oil (mL)** | | **WI** |
|---|---|---|---|---|---|
| **Core no.** | **Spontaneous** ($V_{o1}$) | **Forced** ($V_{o2}$) | **Spontaneous** ($V_{w1}$) | **Forced** ($V_{w2}$) | |
| 1 | 2.80 | 0.05 | 0.00 | 7.20 | 0.98 |
| 2 | 4.50 | 0.10 | 0.00 | 9.00 | 0.98 |
| 3 | 2.70 | 1.00 | 0.00 | 6.80 | 0.73 |

$$\textbf{Wettability Index (WI)} = \frac{V_{o1}}{V_{ot}} - \frac{V_{w1}}{V_{wt}} = r_o - r_w \tag{4.8}$$

Where,

$V_{ot}$ = $V_{o1}$+$V_{o2}$

$V_{wt}$ = $V_{w1}$+$V_{w2}$

**Table 4.4:** Wettability Index chart

| WI range | Wettability |
|---|---|
| +0.3 to +1.0 | Strongly water wet |
| +0.1 to +0.3 | Slightly water wet |
| -0.1 to +0.1 | Neutral |
| -0.3 to -0.1 | Slightly oil wet |
| -1.0 to -0.3 | Strongly oil wet |

Plots of oil displaced (mL) versus time (hours) was established as shown in **Fig. 4.9** and **Fig. 4.10**, where core sample 2 imbibes water hence producing more oil as compared to core sample 1 and 3.

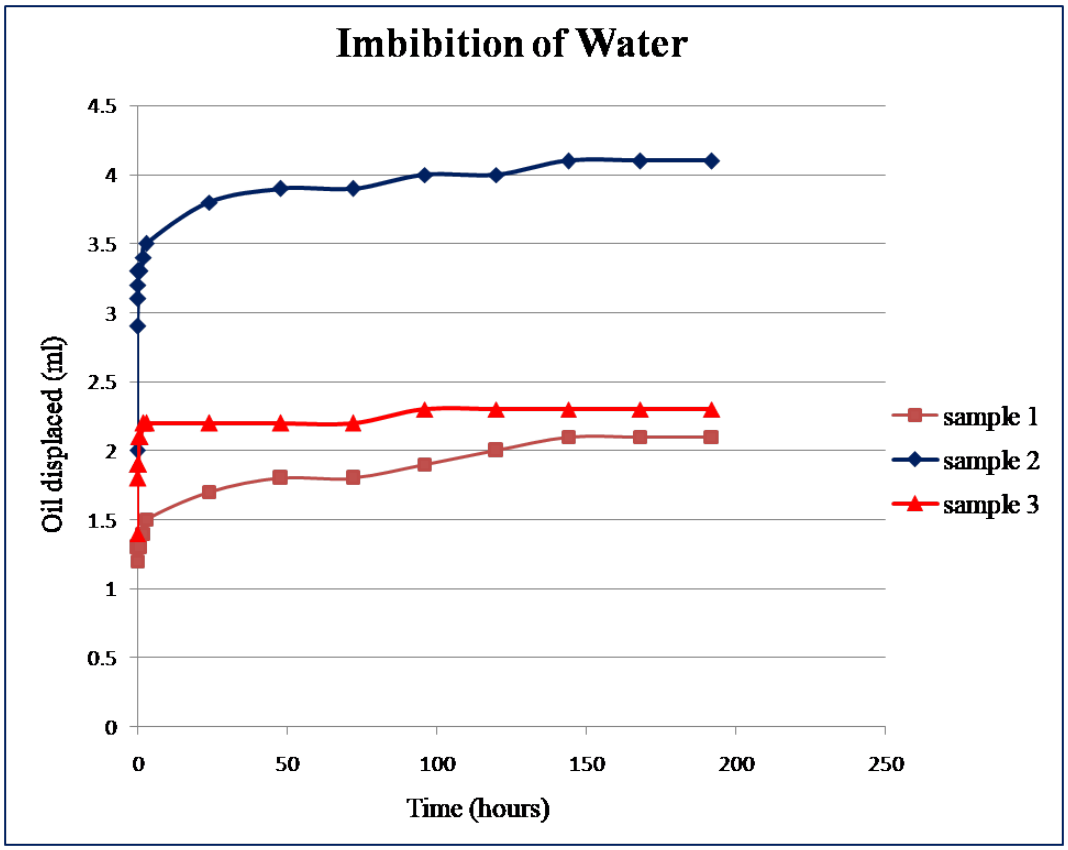


**Figure 4.9:** Production of oil from imbibition of water versus time within 250hours.

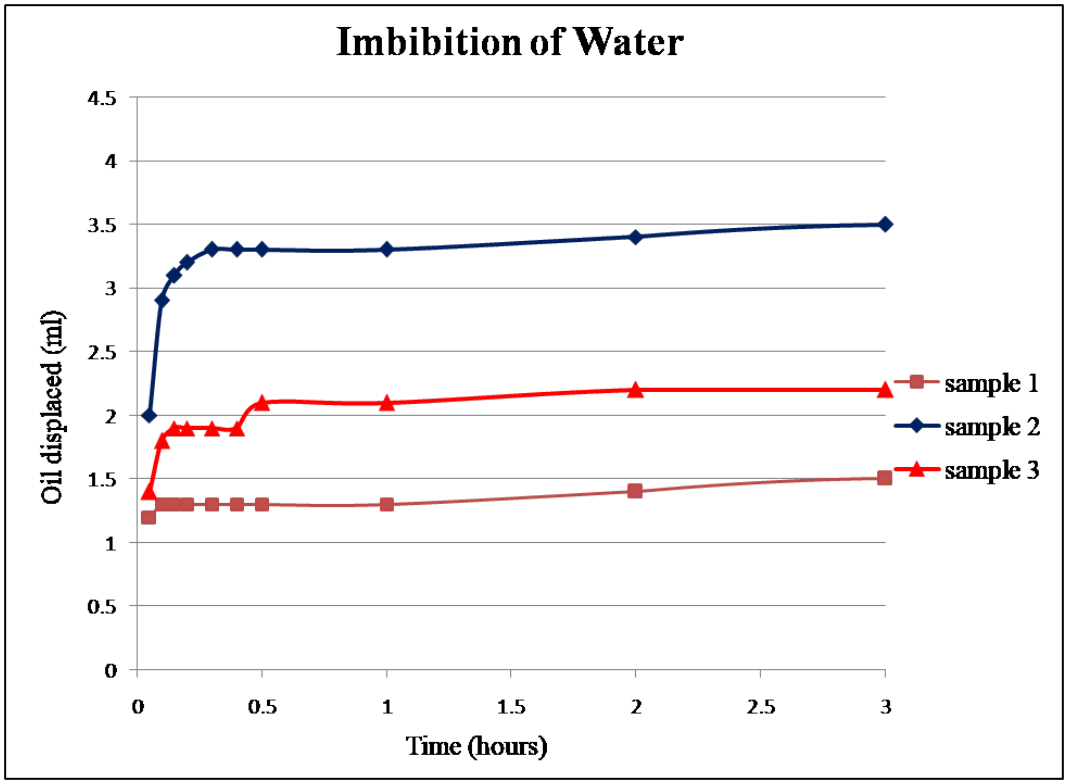


**Figure 4.10:** Production of oil from imbibition of water versus time within 3hours.

The initial (irreducible) water saturation was established for core sample 1, 2 and 3 when centrifuging. The core samples were 100% saturated with water before centrifuging. Initial (irreducible) water saturation (Swi) and oil saturation (Soi) was calculated using the following formula:

$$Swi = \frac{Vp - V_{w2}}{Vp} \tag{4.9}$$

$$Soi = \frac{V_{w2}}{Vp} \tag{4.10}$$

The water saturation (Sw) and oil saturation (So) after water imbibition was calculated accordingly to the following formula:

$$So = \frac{V_{w2} - V_{o1}}{Vp} \tag{4.11}$$

$$Sw = 1 - So \tag{4.12}$$

**Table 4.5:** Water and Oil Saturation Chart

| | | | Water imbibition | | Oil imbibition | |
|---|---|---|---|---|---|---|
| **Core no.** | $S_{oi}$ | $S_{wi}$ | $S_o$ | $S_w$ | $S_o$ | $S_w$ |
| 1 | 0.733 | 0.267 | 0.448 | 0.552 | 0.005 | 0.995 |
| 2 | 0.820 | 0.180 | 0.410 | 0.590 | 0.009 | 0.991 |
| 3 | 0.996 | 0.004 | 0.600 | 0.400 | 0.146 | 0.854 |

Saturation versus time (hours) plots are given in **Fig. 4.11** and **Fig. 4.12**

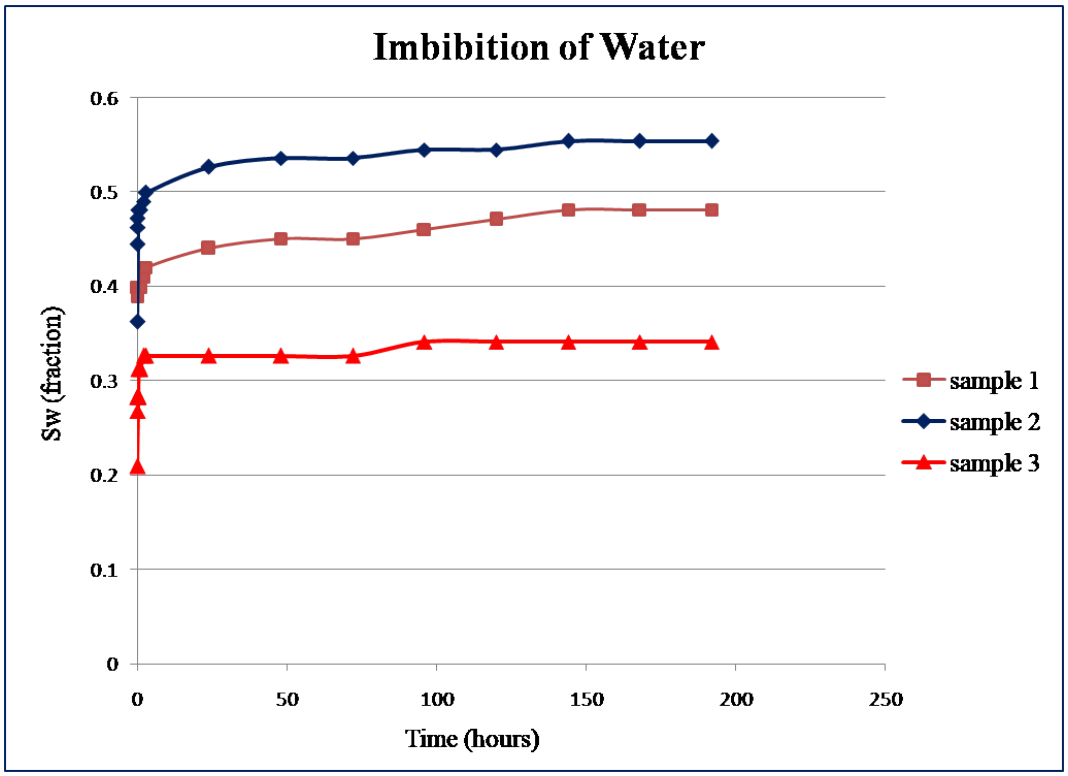


**Figure 4.11:** Water saturation from spontaneous imbibition versus time within 250hours.

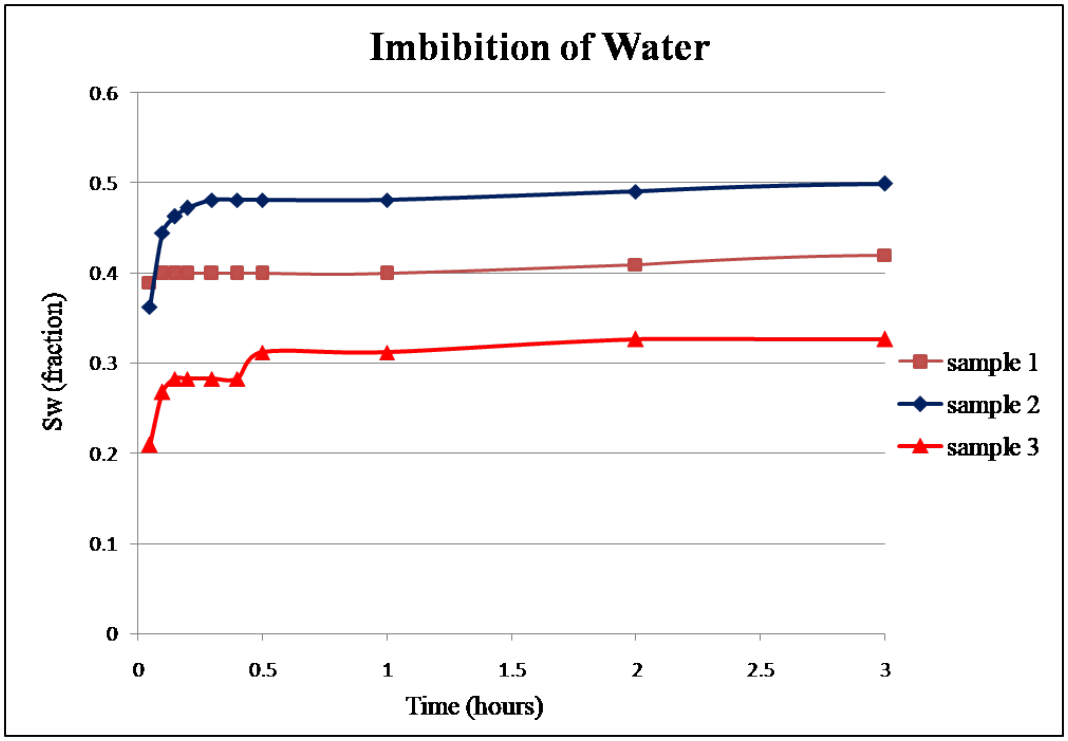


**Figure 4.12:** Water saturation from spontaneous imbibition versus time within 3hours.

## 4.4 Petrographic Analysis

### 4.4.1 Overview of thin section images of samples

Thin sections of the four core samples were analysed and various minerals minerals identified. This analysis was done on Nikon petrographic microscope in PPL (plain polarized light) and XPL (cross polarized light). As discussed in subsection 2.2.1, the following minerals and parameters were determined; Quartz, Feldspar, Rock Fragments, Mica, Quartz Cement, Kaolinite, Primary Porosity and Secondary Porosity. These minerals can be seen in **Figure 4.13, 4.15, 4.16, & 4.17**. The porosity under the crossed polarized light is black because pores optically behave as isotropic and show no birefringence. Under plane polarized light, porosity is seen as blue because the thin section is fixed with epoxy glue which was used to bond the sample to the glass.

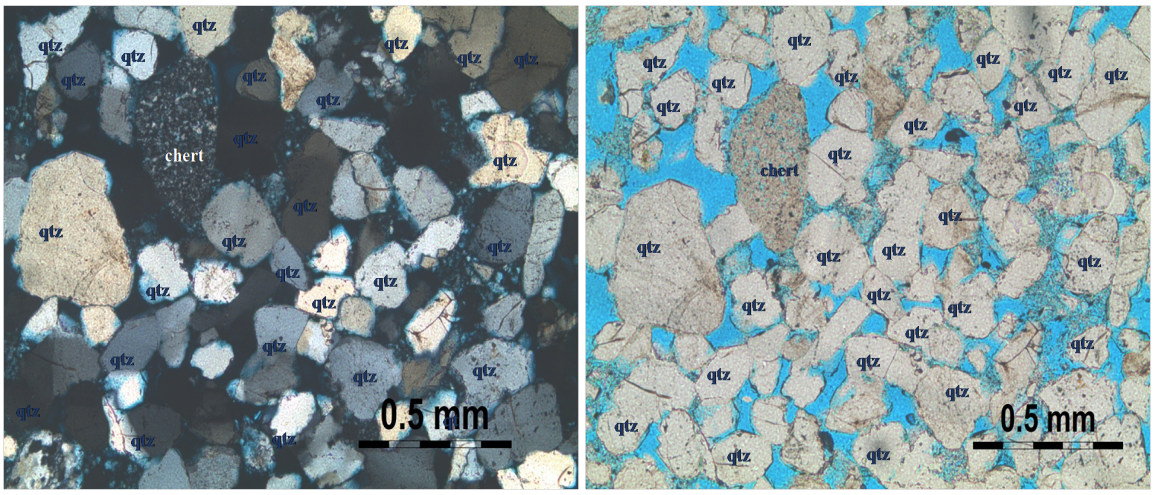


(a) Core sample BSS under plane polarized light (b) Core sample BSS under crossed polarized light

**Figure 4.13:** Thin section of core sample BSS under crossed-polarized and plane-polarized light respectively: qtz=quartz.

Core sample BSS mostly consist of quartz grains, with some quartz cement showing the quartz overgrowth (**Fig. 4.13**). The overgrowth is having a more smoother surface compared to the original quartz grains. The other minor grain constituent in the sample were feldspar, chert and kaolinite (filling the pore space). Secondary porosity was observed in this sample where there is dissolution of feldspar between the quartz grains as seen in **Fig. 4.14**.

Core sample 1 consist of quartz grains with more mica grains with lot of heavy minerals

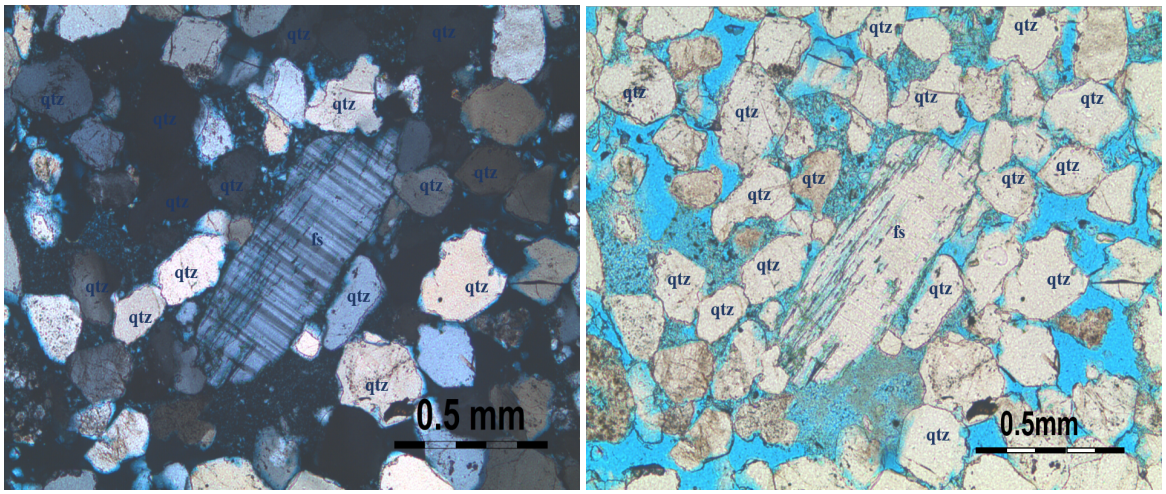


(a) Core sample BSS under plane polarized light (b) Core sample BSS under crossed polarized light

**Figure 4.14:** Thin section of core sample BSS under crossed-polarized and plane-polarized light respectively showing the dissolution of feldspar between the quartz grains: fs=feldspar qtz=quartz.

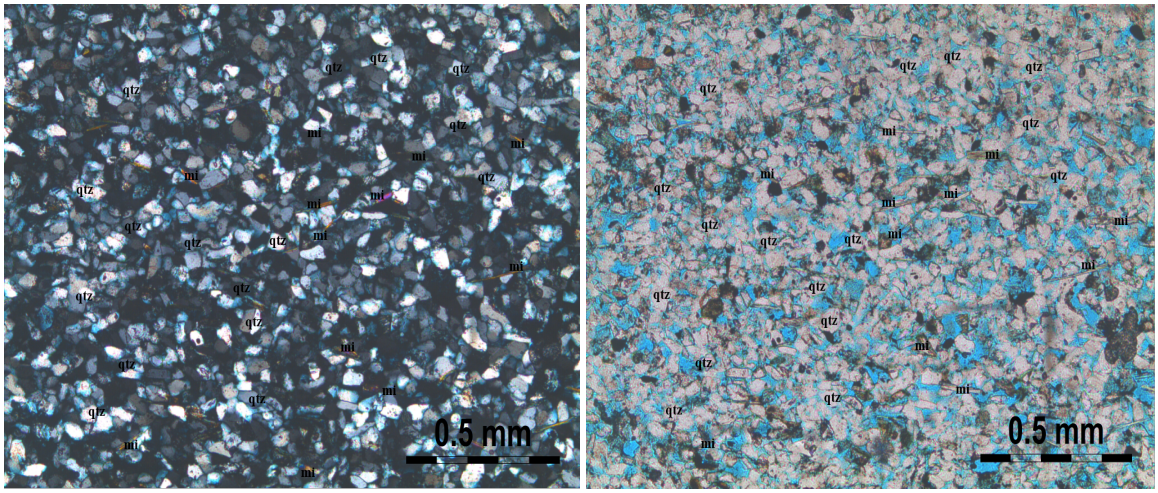


(a) Core sample 1 under plane polarized light (b) Core sample 1 under crossed polarized light

**Figure 4.15:** Thin section of core sample 1 under crossed-polarized and plane-polarized light respectively: mi=mica, qtz=quartz.

in the samples as they appear as black under the plane polarised light as seen in **Fig. 4.15**.

Core sample 2 consist mostly of quartz grains with some displacement of mica between the grains (**Fig. 4.16**). More kaolinite filling the pore space which was confirmed under the SEM technique.

Core sample 3 looks a bit dirty having most of its grains been quartz and some kaolinite filling the pore space. Probably a heavy mineral (zircon) seen at the center of the thin section

as shown in **Fig. 4.17**.

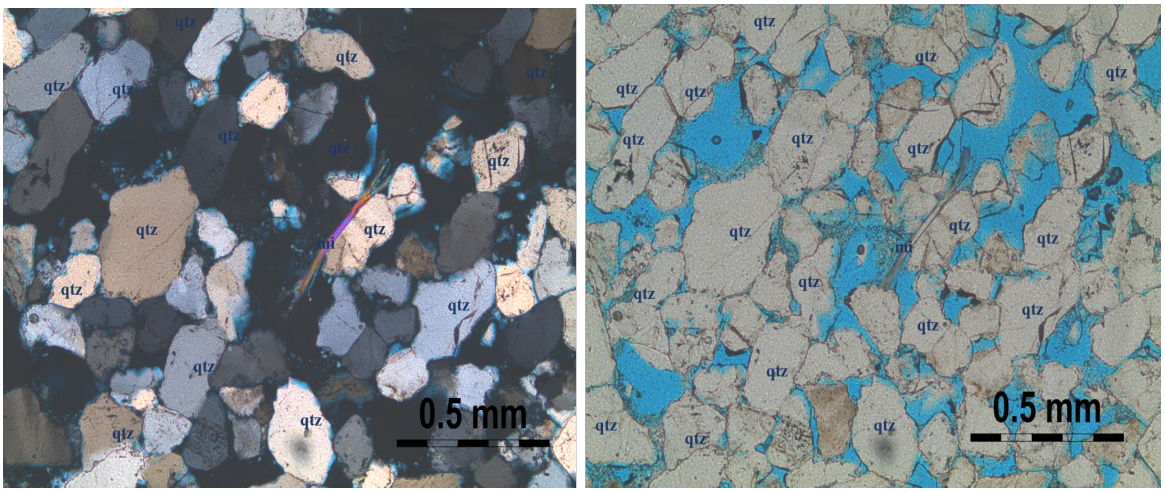


(a) Core sample 2 under plane polarized light (b) Core sample 2 under crossed polarized light

**Figure 4.16:** Thin section of core sample 2 under crossed-polarized and plane-polarized light respectively: mi=mica, qtz=quartz.

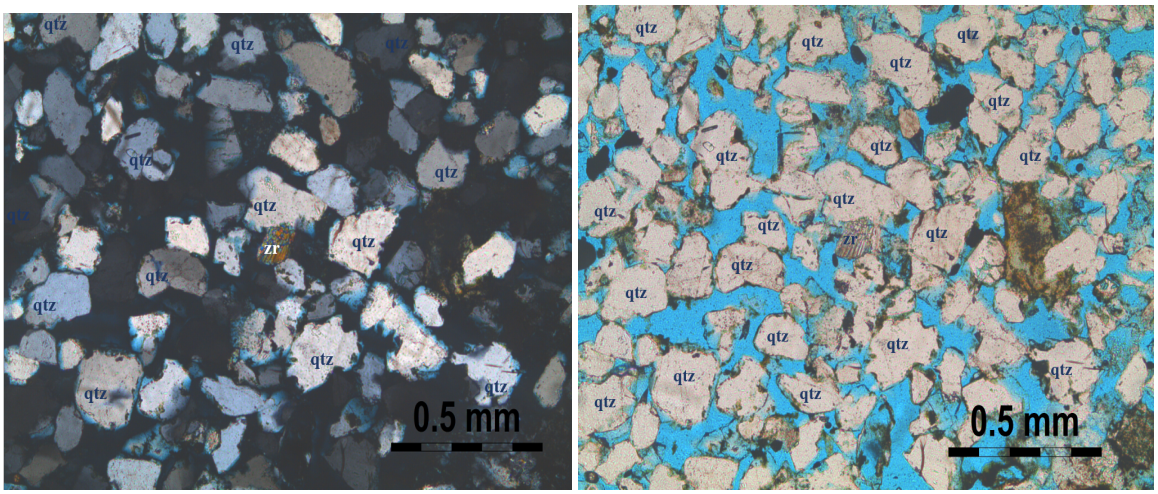


(a) Core sample 3 under plane polarized light (b) Core sample 3 under crossed polarized light

**Figure 4.17:** Thin section of core sample 3 under crossed-polarized and plane-polarized light respectively: mi=mica, qtz=quartz, zr=zircon.

### 4.4.2 Identification of cementing minerals using SEM

Energy dispersive spectra (EDS), can be very useful to calculate the element proportions and the mineral formulas in an unknown sample. The element proportions and mineral formulas of the samples were calculated using the Energy dispersive spectra (EDS), where spectrum displays different peaks. The peak position reflects the energy levels of each element. Each and every element have a standard energy peak. Although the EDS was used to identify the cement, the major minerals were also identified and their formula stated in **Table 4.6** as a reference.

**Table 4.6:** Table of mineral names and their chemical formula.

| **Mineral names** | **Formula** |
|---|---|
| Quartz | $SiO_2$ |
| Muscovite | $K_2Al_4Si_6Al_2O_{20}(OH)_4$ |
| Biotite | $K_2Fe_4Al_2Si_6Al_4O_{20}(OH)_4$ |
| Plagioclase | $NaAlSi_3O_8$-$CaAl_2Si_2O_8$ |
| K-feldspar | $KAlSi_3O_8$ |
| Kaolinite | $Al_2SiO_2O_5(OH)_4$ |

The porosity appear in a black colour on the analysis. This is because porosity is the empty space between the grains and does not contain any mass. Hence, the EDS analysis will not have any energy to reflect and it appears black. The porosity in the samples was mostly intergranualar, but some intragranular porosity was also identified within some of the minerals.

#### Core Sample BSS

**Fig. 4.18 & 4.19** show the EDS diagram of sample BSS where point 5 and 8 having high peaks of aluminium, silicon and oxygen. Which means it is very likely kaolinite grain filling the pore space.

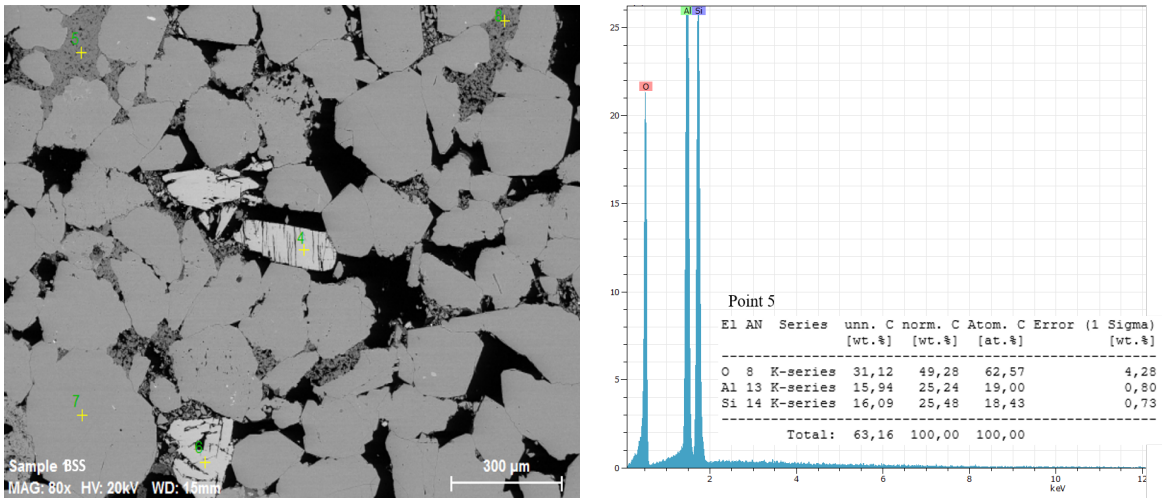


(a) BE-image for sample BSS (b) EDS-diagram for sample BSS showing point 5.

**Figure 4.18:** BE-image for sample BSS and EDS-diagram for point 5.

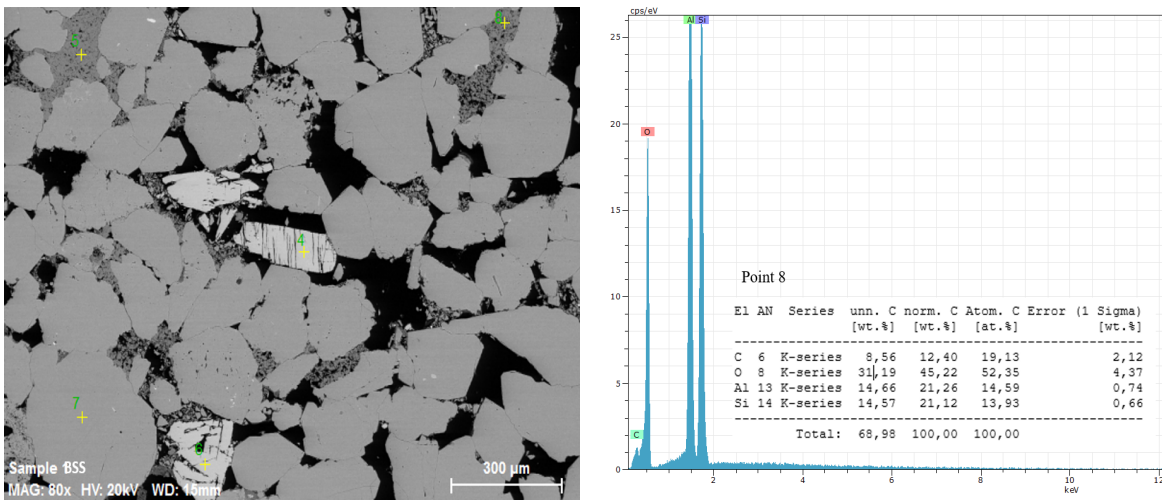


(a) BE-image for sample BSS (b) EDS-diagram for sample BSS showing point 8.

**Figure 4.19:** BE-image for sample BSS and EDS-diagram for point 8

### Core Sample 1

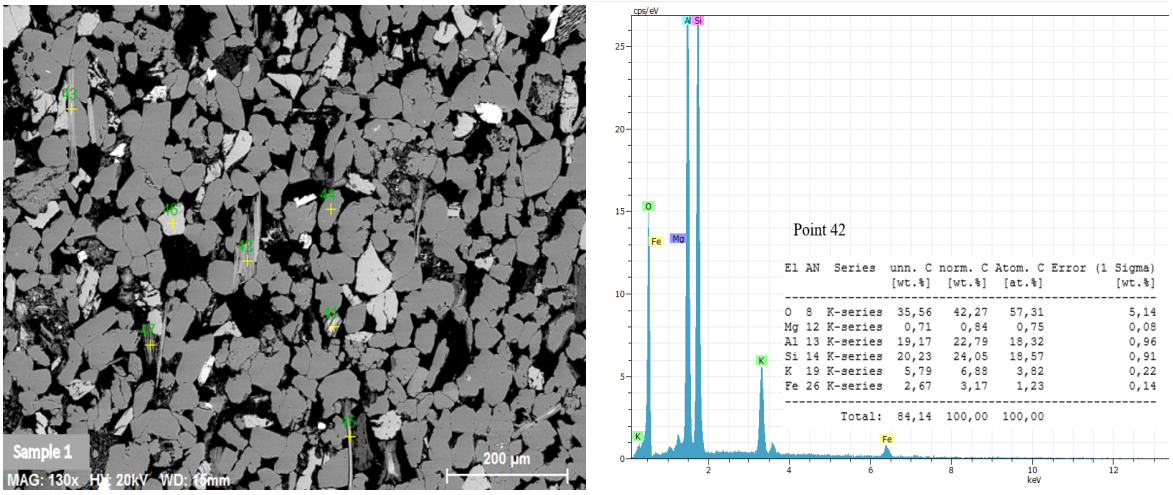


(a) BE-image for sample 1 (b) EDS-diagram for sample 1 showing point 42.

**Figure 4.20:** BE-image for sample 1 and EDS-diagram for point 42.

**Fig. 4.20** show the EDS diagram of sample 1 with high peaks of potassium, aluminium, silicon and oxygen. This is interpreted to be a mica grain probably muscovite, but as there are some smaller peaks of magnesium and iron present. The presence of magnesium and iron suggest the point picked is not pure and might have picked the magnesium and iron from its surrounding.

### Core Sample 2

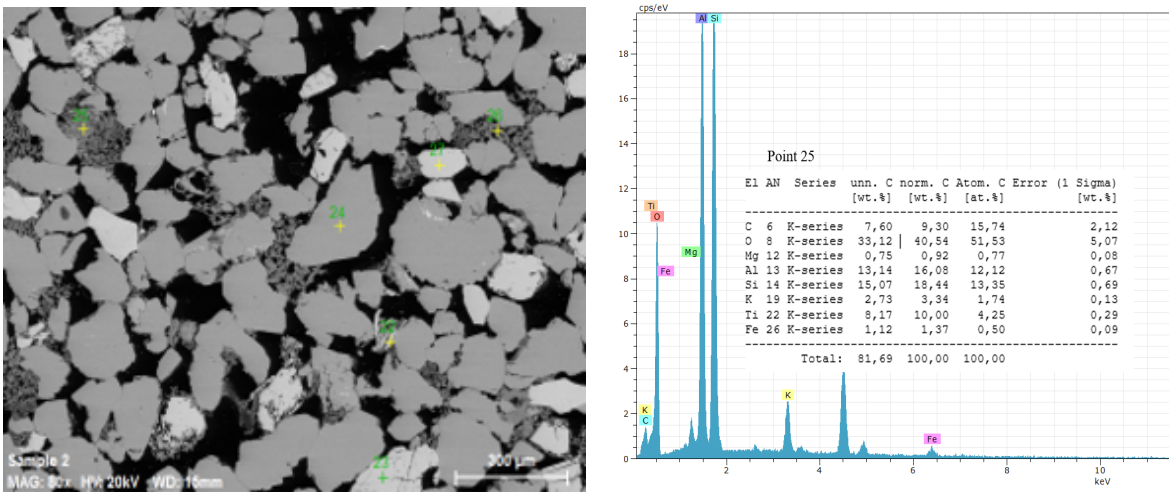


(a) BE-image for sample 2 (b) EDS-diagram for sample 2 showing point 25.

**Figure 4.21:** BE-image for sample 2 and EDS-diagram for point 25.

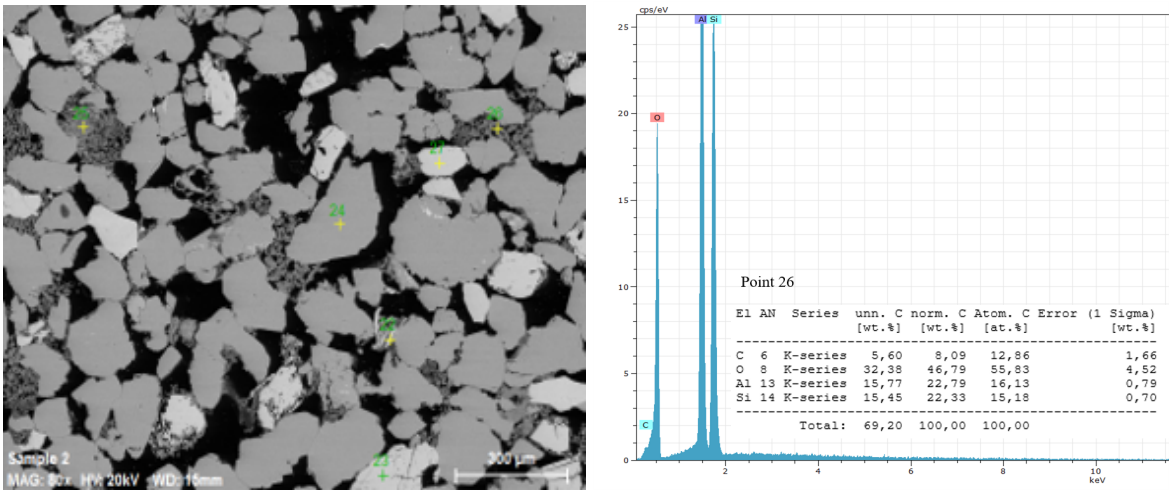


(a) BE-image for sample 2 (b) EDS-diagram for sample 2 showing point 26.

**Figure 4.22:** BE-image for sample 2 and EDS-diagram for point 26.

From **Fig. 4.21 & 4.22**, the BE-images show that sample 2 point 25 and 26 are most likely from an area with cement. Moving to the EDS-diagram, there are very high peaks of aluminum, oxygen and silicon. This combination is most likely kaolinite cement. However, **Fig. 4.21** is having some smaller peaks of magnesium, iron and titanium in addition to aluminum, oxygen and silicon. This might be as a result of the surrounding minerals.

### Core Sample 3

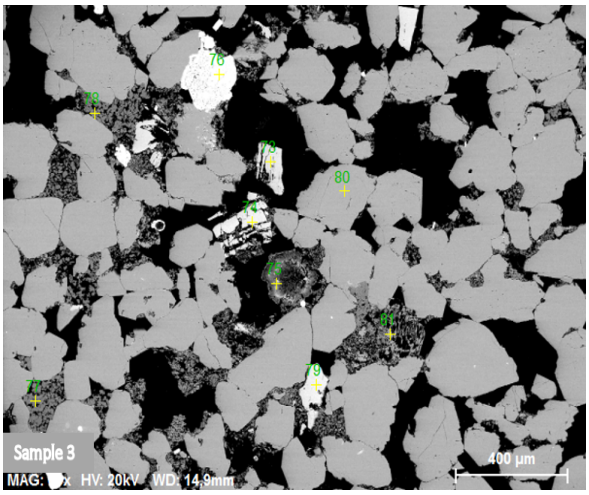


(a) BE-image for sample 3

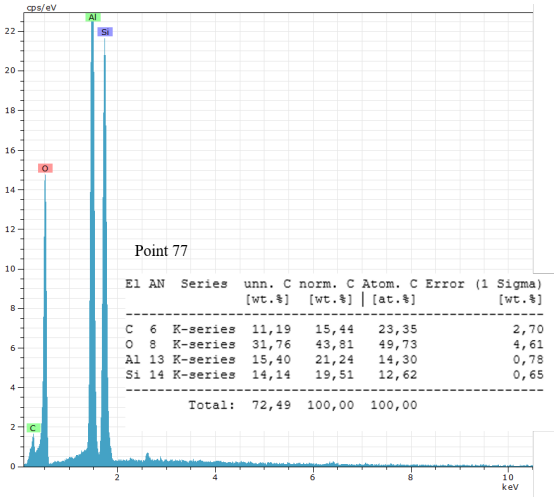


(b) EDS-diagram for sample 3 showing point 77.

**Figure 4.23:** BE-image for sample 3 and EDS-diagram for point 77.

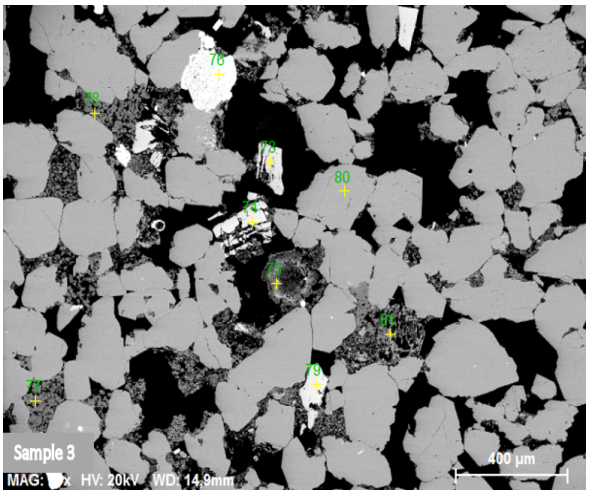


(a) BE-image for sample 3

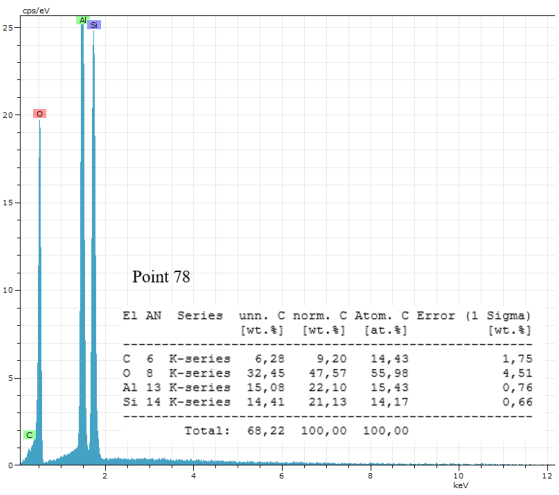


(b) EDS-diagram for sample 3 showing point 78.

**Figure 4.24:** BE-image for sample 3 and EDS-diagram for point 78.

**Fig. 4.23 & 4.24**, the BE-images show that sample 3 point 77 and 78 are most likely from an area with cement having very high peaks of aluminum, oxygen and silicon. This combination is most likely kaolinite cement.

Chapter 5

# Discussion

## 5.1 Porosity Determination Methods

Porosity can be determined by various methods, both in the laboratory and by petrographic image analysis. Laboratory determination of porosity were carried out in this experiment. However, the porosity values obtained by the various laboratory methods might not be the same. Porosity determined in the laboratory is not influenced by the mineralogical composition of the sample but thin section estimation of porosity is influenced by the mineralogical composition of the sample.

Accordingly to Cone and Kersey (1992), the four basic types of porosity that can be recognized in sandstone are intergranular (primary), microporosity, dissolution (secondary) and fracture as shown in **Fig. 5.1**. Most of the porosity type found in the four samples used for this experiment are intergranular with few dissolution (secondary) porosity. This type of dissolution porosity can be seen in core sample BSS as shown in **Fig. 4.13**.

### 5.1.1 Comparison Between the Porosity Determination Methods

Porosity values of a given sample may vary due to the various methods used in the porosity determination. The Boyle's law porosity which is determined using the measured grain volume from the helium porosimeter in the laboratory. This type of porosity measurement is accurate and not sensitive to rock mineralogy and can be easily measured after cleaning and drying the core sample. Cone and Kersey (1992) further discussed how the porosity

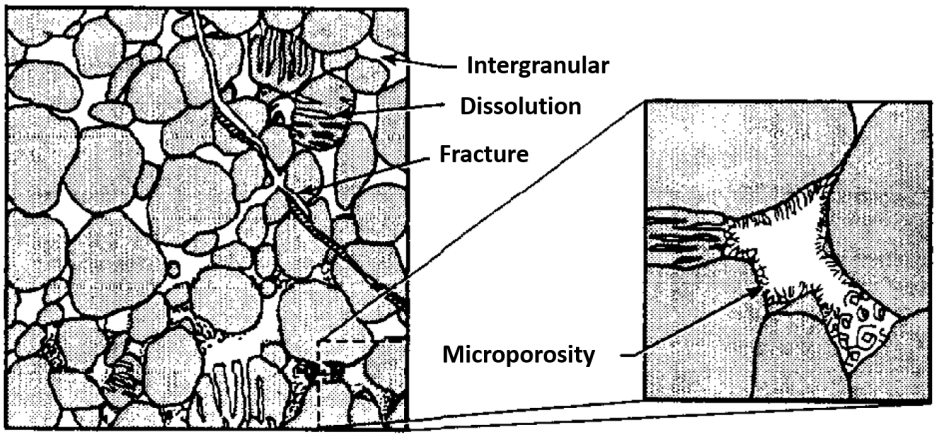


**Figure 5.1:** Four basic types of porosity in sandstone (Cone and Kersey, 1992).

values of a sample can vary due to the technique used to dry the core sample if the rock contain smectite. Thus, the oven-dried total porosity will be larger than the humidity-dried total porosity.

The saturation time is dependent on rock permeability when using liquid saturation method for porosity determination. This can be observed in core sample 2 where permeability value is high due to a good interconnectivity of pores (**Fig. 4.6**), thereby may saturate more easily or faster.

Precise determination of visible porosity and porosity types can be determined on fracture and irregular samples by the petrographic image analysis.

## 5.2 Textural Parameters Controlling Petrophysical Properties

Many researcher such as (Slatt, 2013; Beard and Weyl, 1973; Fraser, 1935) have shown that porosity and permeability are strongly influenced by the textural properties of sediments (**Fig. 5.2**). Although, grain sorting or the uniformity of grain size, grain packing, grain shape (sphericity) and roundness (angularity) may have a pronounced effect on porosity and permeability; textural and mineralogical maturity have pronounced effect on petrophysical properties.

Although ductile detrital minerals such as mica and clays may cause a significant loss in

porosity by blocking interparticle pores, more stable minerals or rigid grains such as quartz and feldspar are more likely to bear the overburden pressure and as a result may preserve primary interparticle pores.

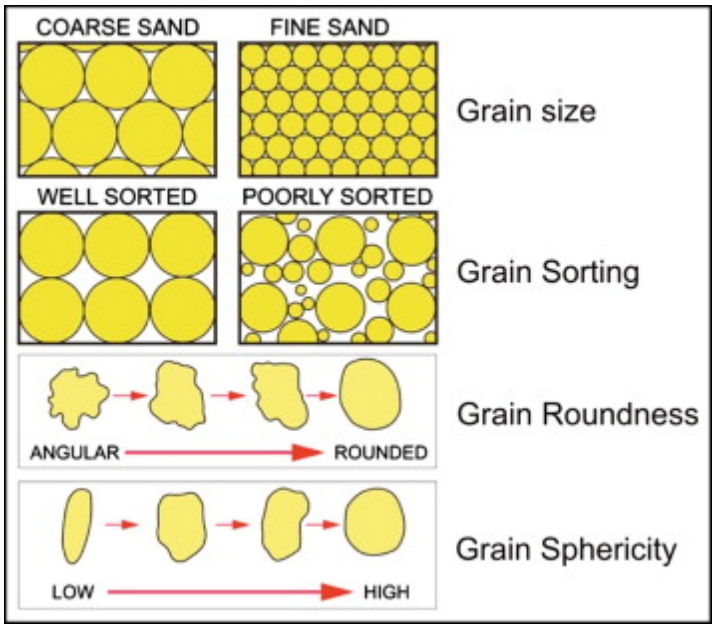


**Figure 5.2:** Textural properties of clastic sediments (Slatt, 2013).

According (Cone and Kersey, 1992), porosity might decrease as a result of the sphericity of grains increasing. This is due to the spherical grains mostly associated with having a tighter packing arrangement.

A well sorted sand is considered as texturally matured and a mineralogically (compositional) matured sandstone consist of a higher percentage of more stable minerals such as quartz. Sorting is also an important attribute which influences the porosity, as seen **Fig. 4.16**, sample 2 is having a higher porosity of 27% (**Table 4.1**) as a result of it being well sorted and mineralogically matured.

## 5.3 Rock Wettability and its instability

Wettability is the tendency of a fluid to adhere to the surface of a solid in the presence of another fluid, and this is the major factor that controls the distribution of fluid in a porous medium (Donaldson et al., 1969; Anderson et al., 1987). The three core samples (1, 2 and 3) were determined to be moderately water wet to strongly water wet. The Amott wettability

index (WI) values were 0.73 to 0.98. The wetting conditions of the samples can be seen in **Fig. 4.10** and **Fig. 4.12**. where steeper slope in the initial hours during the imbibition is interpreted as water wet. During the wettability measurements, irreducible fluid saturations as well as the fluid saturation were also determined. There is a good relationship between the fluid saturation, absolute permeability and the wettability characteristics of the core samples. The permeability values of the strongly water wet sample was higher than the moderately water wet sample. However, core sample 1 which was strongly water wet had a lower permeability compared to the core sample 3 which was moderately water wet. This could be caused by the interconnectivity of the pore and the pore size distribution of the core sample (Morgan et al., 1970).

Inconsistency in the results of tests on a core material with the results of other cores from same reservoir may be due to the changes in wettability of the core before or during the test (Bobek et al., 1958). This changes may result from the core storage or while handling the core material.

## 5.4 Effect of Textural Properties and Mineralogy on Wettability

Worden et al. (1998) researched to show that quartz is normally water-wet as observed in core sample 2 and produces more oil as shown in **Fig. 5.3**. This means that quartz is considered unlikely to come into direct contact with oil, even though there were some cement that might have precipitated and some amount of alkali feldspar in the core sample.

Core sample 1, having more mica mineral content than the stable quartz mineral, have some impact on its ability to imbibe more water in the Amott cell test (**Fig. 4.9**), hence producing lower volume of oil.

Although core sample 1 having a high pore volume and a higher wettability index (0.98) with an average contact angle ($\theta < 90°$) as compared to the other core sample as shown in **Fig. 5.4**. As clearly seen in **Fig. 5.5**, the oil makes contact with the sample surface in the presence of water but it wasn't able to imbibe water during the Amott cell test as seen in **Fig. 4.11**.

On the other hand, core sample 2 also have a high pore volume with a high wetting index

of 0.98, which is interpreted to be strongly water wet and could imbibe more water as seen in **Fig. 4.11**. This may be due to the high percentage of quartz mineral as compared to the other core sample. This wetting condition can clearly be seen in **Fig. 4.10**, where core sample 2 produces more oil within 3hours and continue to produce. **Fig. 4.12** also shows how core sample 2 continue to imbibe water after 3hours as compared to core sample 1 and 3.

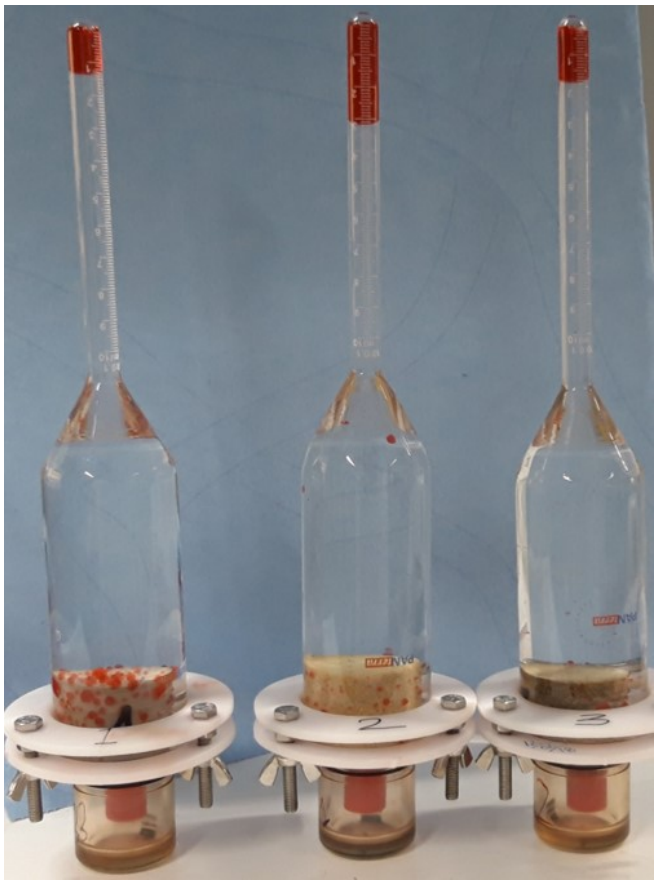


**Figure 5.3:** The three(3) core samples displaced in Amott cell at the laboratory, sample core 1, 2, 3 respectively.

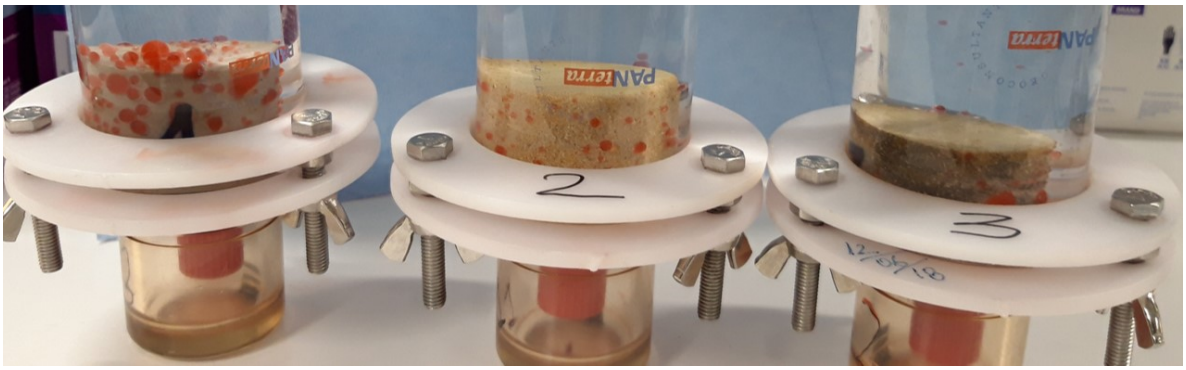


**Figure 5.4:** The wetting condition of the core sample 1, 2, 3 respectively.

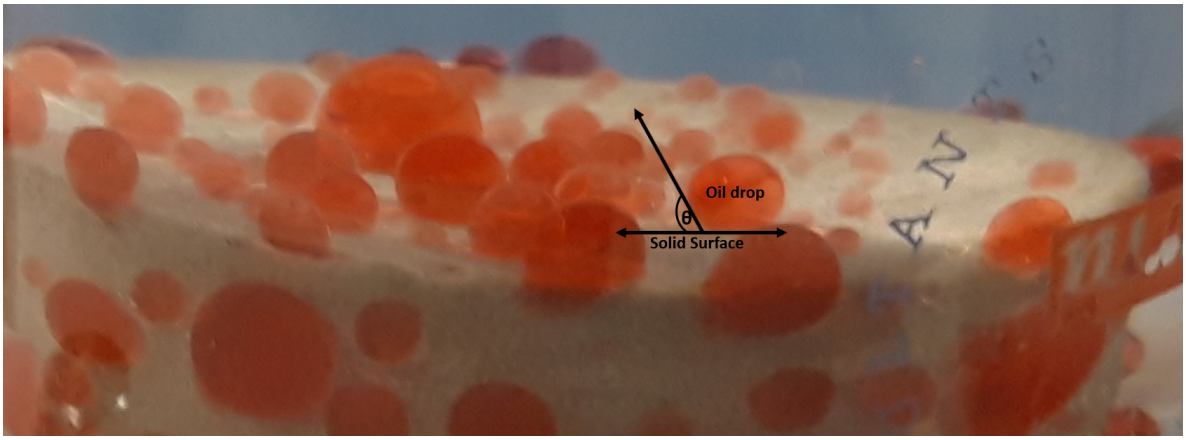


**Figure 5.5:** The wetting condition of the core sample 1.

Chapter 6

# Conclusion and Recommendation

**Conclusion**

Sandstones are made of different minerals but few are essential. By observing images of thin sections viewed under a polarizing microscope, these essential minerals in the rock samples can be identified. The Scanning electron microscope (SEM) is an important tool which helps to provide information as well as evaluating the clay minerals. Chemical composition using energy-dispersive X-ray attachment for the SEM in combination with Backscattered electron imaging helps in the identification of minerals.

Porosity can be estimated by several methods for which different values may be obtained from same core sample. Core samples with high pore volume leading to a higher value for porosity do not necessarily have a higher permeability value. This can be the influence of textural properties such as the distribution of grain size, grain shape and grain packing. Although core sample 1 have a high porosity value of 24% but was having the least absolute permeability value of 23.3mD.

The wettability of the reservoir surface is an important factor in the efficiency of the oil recovery process. However, the Amott cell method can be used to estimate the average wettability index of a core sample which gives the wetting condition of that sample than an individual mineral.

Different mineral and their characterises affect the wetting condition of a core sample. Quartz minerals seems to be more water wet as compared to the other essential minerals. Core sample 2 with a higher amount of quartz is more water wet from the experiment which confirms the wetting nature of quartz mineral.

**Recommendation**

This research was conducted based on four (4) core samples, and wettability experiment on only three (3) core samples. Four core samples is not enough to conduct a thorough experiment and conclude based on the experiment, since a core sample of same mineral composition and properties but might end up with different findings. An appreciable number of core samples of 20 or more might be accurate to conclude on this research finding.

# References

Abdallah, W., Buckley, J. S., Carnegie, A., Edwards, J., Herold, B., Fordham, E., Graue, A., Habashy, T., Seleznev, N., Signer, C., et al., 1986. Fundamentals of wettability. Technology 38 (1125-1144), 268.

Adams, A. E., MacKenzie, W. S., Guilford, C., 2017. Atlas of sedimentary rocks under the microscope. Routledge.

Amott, E., 1959. Observations relating to the wettability of porous rock. Society of Petroleum Engineers, 156–162.

Anderson, W. G., et al., 1987. Wettability literature survey part 5: the effects of wettability on relative permeability. Journal of Petroleum Technology 39 (11), 1453–1468.

Beard, D. C., Weyl, P. K., 1973. Influence of texture on porosity and permeability of unconsolidated sand. AAPG Bulletin 57 (4), 349–369.

Bjørlykke, K., 2010. Petroleum geoscience: From sedimentary environments to rock physics. Springer Science & Business Media.

Bloch, S., 1991. Empirical prediction of porosity and permeability in sandstones. AAPG Bulletin 75 (7), 1145–1160.

Bobek, J., Mattax, C., Denekas, M., et al., 1958. Reservoir rock wettability-its significance and evaluation. Society of Petroleum Engineers, 156–160.

Charles, Merguerian, J. M., 2014. Field Trip Guidebook Isham and Inwood Parks, NYC. Lamont-Doherty Earth Observatory Manhattan Prong Workshop, 06-07 September.

Cone, M. P., Kersey, D. G., 1992. Porosity: Part 5. laboratoy methods. AAPG Special Volumes.

Dabbs, D. M., Mulders, N., Aksay, I. A., 2006. Solvothermal removal of the organic template from l 3 ("sponge") templated silica monoliths. Journal of Nanoparticle Research 8 (5), 603–614.

Donaldson, E. C., Thomas, R. D., Lorenz, P. B., et al., 1969. Wettability determination and its effect on recovery efficiency. Society of Petroleum Engineers Journal 9 (01), 13–20.

Dyar, M. D., Gunter, M. E., Tasa, D., 2008. Mineralogy and optical mineralogy. Mineralogical Society of America Chantilly, VA.

Earle, S., 2018. Physical geology. licensed under a Creative Commons Attribution 4.0 International License.

Fraser, H. J., 1935. Experimental study of the porosity and permeability of clastic sediments. The Journal of Geology 43 (8, Part 1), 910–1010.

Gant, P. L., Anderson, W. G., et al., 1988. Core cleaning for restoration of native wettability. SPE formation evaluation 3 (01), 131–138.

Graton, L. C., Fraser, H., 1935. Systematic packing of spheres: with particular relation to porosity and permeability. The Journal of Geology 43 (8, Part 1), 785–909.

Haldar, S. K., 2013. Introduction to mineralogy and petrology. Elsevier.

Kandarpa, V., Sparrow, J. T., et al., 1981. A useful technique to study particle invasion in porous media by backscattered electron imaging. In: SPE Annual Technical Conference and Exhibition. Society of Petroleum Engineers, pp. 1–7.

Lander, R. H., Walderhaug, O., 1999. Predicting porosity through simulating sandstone compaction and quartz cementation. AAPG bulletin 83 (3), 433–449.

MacKenzie, W. S., Guilford, C., 2014. Atlas of the Rock-Forming Minerals in Thin Section. Routledge.

Morgan, J., Gordon, D., et al., 1970. Influence of pore geometry on water-oil relative permeability. Journal of Petroleum Technology 22 (10), 1–199.

Niazia, A. M. K., Jahren, J., Mahmood, I., Javaid, H., 2019. Reservoir quality in the Jurassic sandstone reservoirs located in the Central Graben, North Sea. Marine and Petroleum Geology 102, 439-454.

Nichols, G., 2009. Sedimentology and stratigraphy. John Wiley & Sons.

Oyeneyin, B., 2015. Introduction to the hydrocarbon composite production system. In: Developments in Petroleum Science. Vol. 63. Elsevier, pp. 11–128.

Slatt, R. M., 2013. Chapter 2 - basic sedimentary rock properties. In: Slatt, R. M. (Ed.), Stratigraphic Reservoir Characterization for Petroleum Geologists, Geophysicists, and Engineers. Vol. 61 of Developments in Petroleum Science. Elsevier, pp. 39 – 93.

Tiab, D., Donaldson, E. C., 2015. Petrophysics: theory and practice of measuring reservoir rock and fluid transport properties. Gulf professional publishing.

Torsæter, O., Abtahi, M., 2003. Experimental reservoir engineering laboratory workbook. Department of Petroleum Engineering and Applied Geophysics, Norwegian University of Science and Technology (NTNU), Trondheim.

West, J., 1985. Toward an expert system for identification of minerals in thin section. Journal of the International Association for Mathematical Geology 17 (7), 743–753.

Worden, R. H., Oxtoby, N. H., Smalley, P. C., 1998. Can oil emplacement prevent quartz cementation in sandstones? Petroleum Geoscience 4 (2), 129–137.

Yuan, Y., Lee, T. R., 2013. Contact angle and wetting properties. In: Surface science techniques. Springer, pp. 3–34.

# Appendix

# Methodology

**Helium Porosimeter**

Detailed description of how volume of matrix cup with core ($V_2$) was determined is as follows:

1. The cleaned dried core was placed inside the matrix cup and mounted in cup holder.
2. Open "source" followed by "supply".
3. The needle was regulated to 100.
4. "Source" and "supply" were closed consecutively.
5. "Core holder" was opened.
6. Reading was taken from the top scale as $V_2$ in $cm^3$.

.

Detailed description of how thee volume of matrix cup without core ($V_1$) was determined is as follows:

1. The cleaned dried core was taken out of the matrix cup and mounted in cup holder.
2. Open "source" followed by "supply".
3. "Cell 1" was opened.
4. The needle was regulated to 100.
5. "Source" and "supply" were closed consecutively.

6. "Core holder" was opened.

7. Reading was taken from the middle scale as $V_1$ in $cm^3$.

## Core Sample BSS

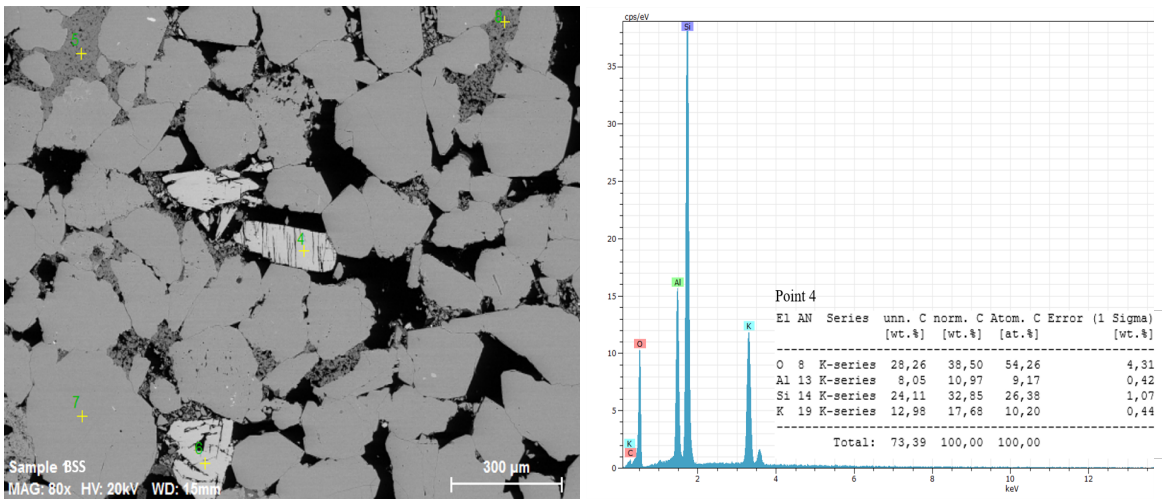


(a) BE-image for sample BSS (b) EDS-diagram for sample BSS showing point 4.

**Figure 6.1:** BE-image for sample BSS and EDS-diagram for point 4.

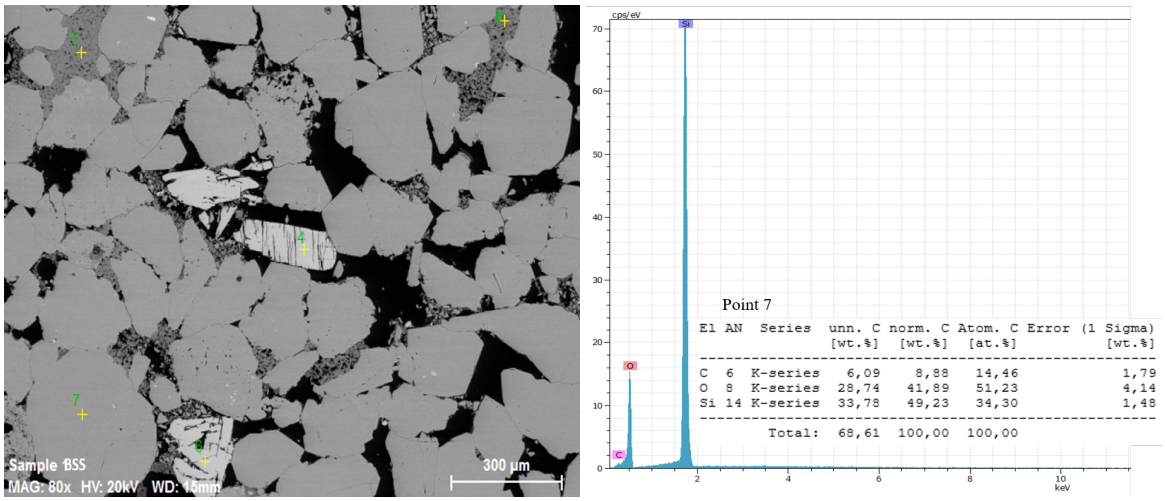


(a) BE-image for sample BSS (b) EDS-diagram for sample BSS showing point 7.

**Figure 6.2:** BE-image for sample BSS and EDS-diagram for point 7

**Fig. 6.1(b) & 6.2(b)** The EDS spectra shows high peaks of both silicon and oxygen, which means it is very likely a quartz grain.

## Core Sample 2

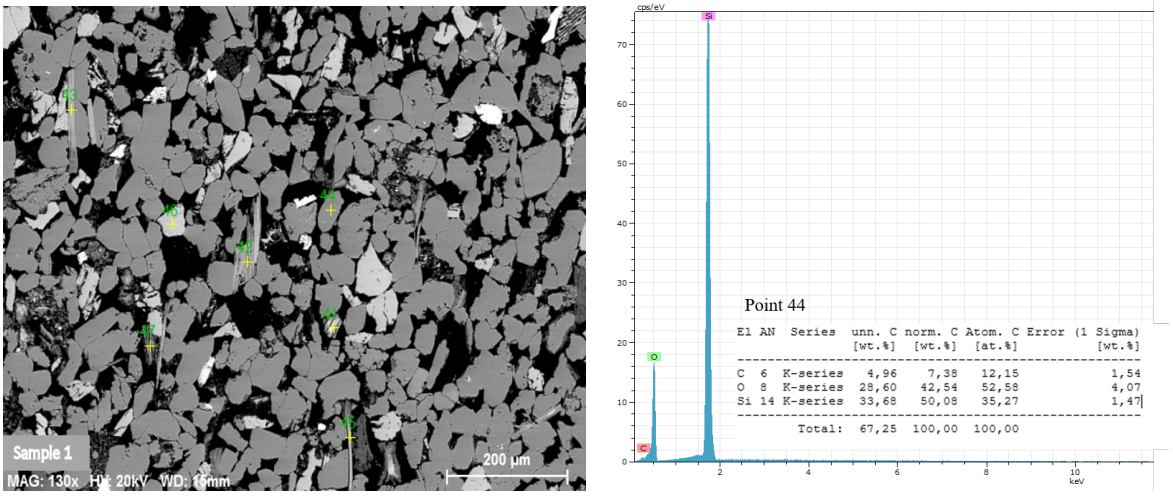


(a) BE-image for sample 1 (b) EDS-diagram for sample 1 showing point 44.

**Figure 6.3:** BE-image for sample 1 and EDS-diagram for point 44 (quartz).

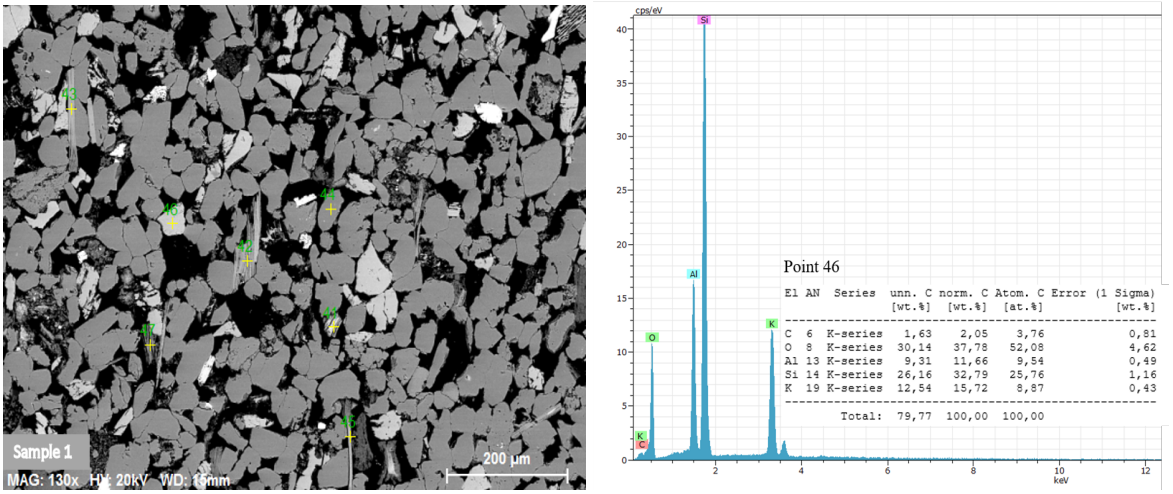


(a) BE-image for sample 1 (b) EDS-diagram for sample 1 showing point 46.

**Figure 6.4:** BE-image for sample 1 and EDS-diagram for point 46 (feldspar).

## Core Sample 2

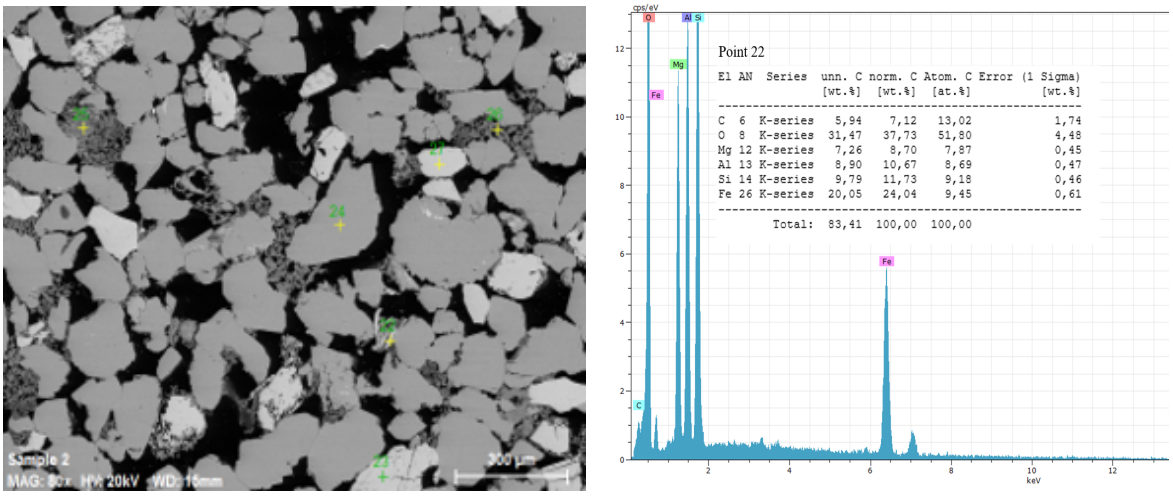


(a) BE-image for sample 2 (b) EDS-diagram for sample 2 showing point 22.

**Figure 6.5:** BE-image for sample 2 and EDS-diagram for point 22 (mica).

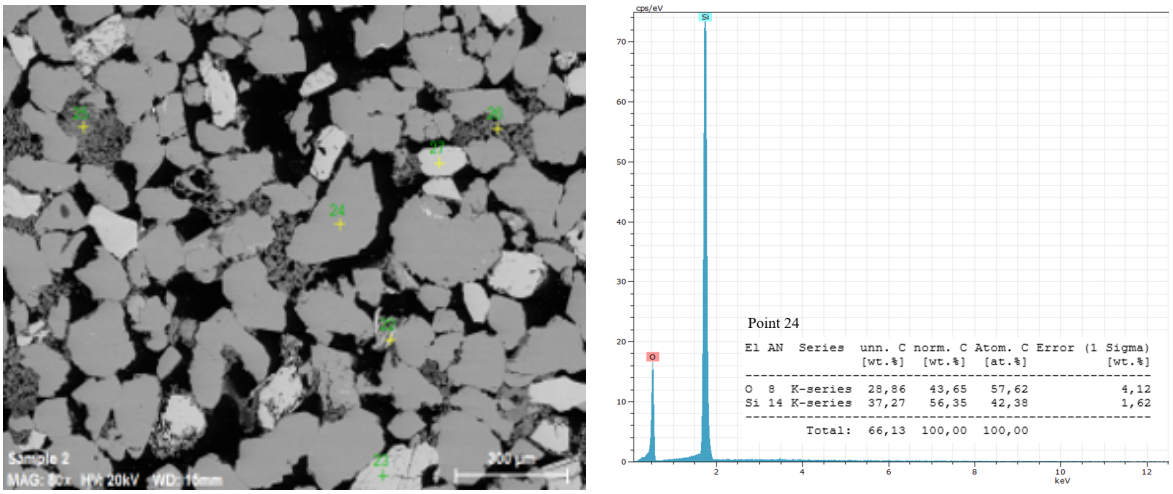


(a) BE-image for sample 2 (b) EDS-diagram for sample 2 showing point 24.

**Figure 6.6:** BE-image for sample 2 and EDS-diagram for point 24 (quartz).

## Core Sample 3

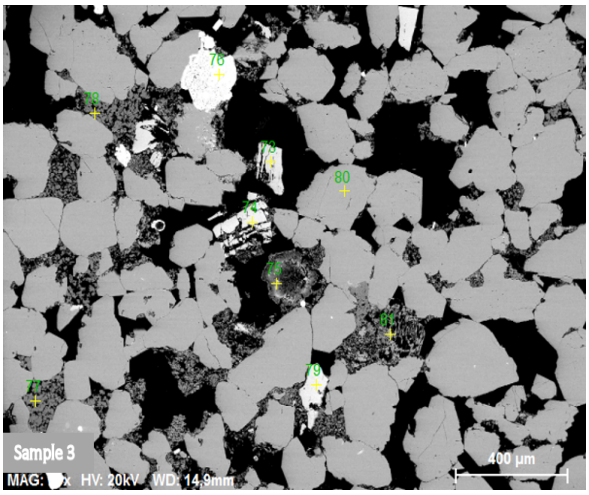


(a) BE-image for sample 3

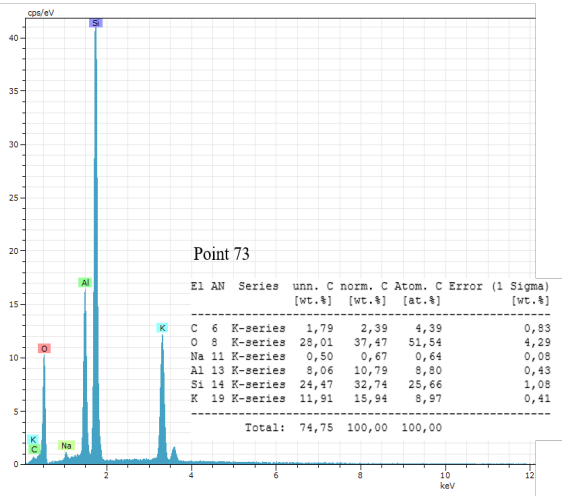


(b) EDS-diagram for sample 3 showing point 73.

**Figure 6.7:** BE-image for sample 3 and EDS-diagram for point 73 (plagioclase).

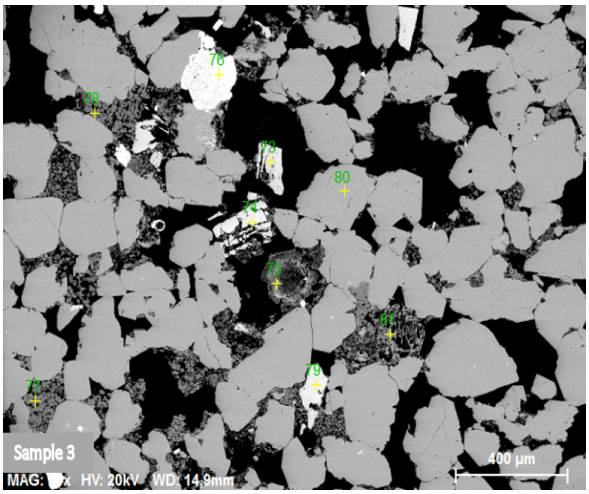


(a) BE-image for sample 3

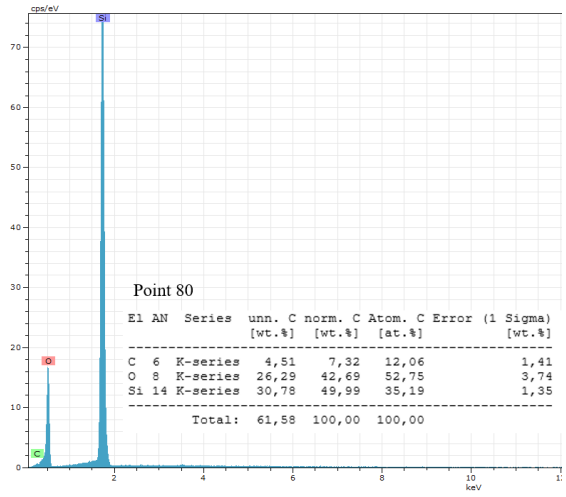


(b) EDS-diagram for sample 3 showing point 80.

**Figure 6.8:** BE-image for sample 3 and EDS-diagram for point 80 (quartz).

NTNU
Norwegian University of
Science and Technology